TAMPEREEN TEKNILLINEN YLIOPISTO
TAMPERE UNIVERSITY OF TECHNOLOGY
*Julkaisu 741 • Publication 741*

Outi Väisänen

# Multichannel EEG Methods to Improve the Spatial Resolution of Cortical Potential Distribution and the Signal Quality of Deep Brain Sources

Tampere 2008

Tampereen teknillinen yliopisto. Julkaisu 741
Tampere University of Technology. Publication 741

Outi Väisänen

# Multichannel EEG Methods to Improve the Spatial Resolution of Cortical Potential Distribution and the Signal Quality of Deep Brain Sources

Thesis for the degree of Doctor of Technology to be presented with due permission for public examination and criticism in Rakennustalo Building, Auditorium RG202, at Tampere University of Technology, on the 13th of June 2008, at 12 noon.

Tampereen teknillinen yliopisto - Tampere University of Technology
Tampere 2008

ISBN 978-952-15-1986-4 (printed)
ISBN 978-952-15-1999-4 (PDF)
ISSN 1459-2045

## ABSTRACT

Electroencephalography (EEG) is a convenient technique for studying the function of the brain non-invasively from the surface of the scalp. The greatest advantages of EEG are its temporal resolution on a millisecond scale and its affordability compared to other non-invasive techniques employed to register brain activity. The development in amplifier technology, computerized signal processing methods and modern EEG caps make the application of multichannel EEG systems a feasible objective. Nowadays measurement systems of up to 256 electrodes and over are available. It is thus important to evaluate the benefits obtained with the multichannel systems when different functions of the brain are being studied.

In this thesis two opposite applications of multichannel EEG are investigated. The first of these deals with superficial sources and concerns improving the spatial resolution of inverse cortical potential distribution. The other application concerns the modification of the measurement sensitivity distributions of EEG leads to improve the signal-to-noise ratio (SNR) of signals generated deep within the brain.

When studying the spatial resolution of cortical potential distribution, special attention was given to an examination of the effect of measurement noise and relative skull resistivity on the estimation of accuracy of the inverse solution. A three-layer spherical head model was applied with new realistic estimates for skull resistivity. The measurement noise levels were estimated in realistic measurement environments, bearing in mind that when the cortical potential distribution is studied as a solution of the inverse problem, the entire brain activity is considered as the desired signal. The results of the theoretical evaluation show that with the new realistic estimates for relative skull resistivity, the application of up to 128 - 256 electrodes improves the spatial resolution of cortical potential distribution.

To improve the SNR of signals generated by deep EEG sources, multielectrode EEG leads were developed. Theoretically a multielectrode EEG lead consists of two terminals, which are both connected through a resistor network to several electrodes on the surface of the scalp. Reciprocity and lead field theorems were applied to modify the sensitivity distribution of a multielectrode lead to be optimal for deep brain sources. The results of preliminary experimental evaluation conducted by studying brainstem auditory evoked potentials show that with a multielectrode EEG lead consisting of 114 electrodes, it is sufficient to average 45 % of the number of epochs needed with bipolar leads to obtain a similar SNR. The results of the theoretical study demonstrate that further improvements can be obtained by such steps as optimizing the electrode positions.

# ACKNOWLEDGEMENTS

The work for the thesis was carried out at the Ragnar Granit Institute, Department of Electrical Engineering, Tampere University of Technology. Due to structural reform at Tampere University of Technology, the work was finalized at the new Department of Biomedical Engineering.

I wish to express my gratitude to my supervisor, Professor Jaakko Malmivuo, PhD, for his guidance throughout this research; his expertise in bioelectromagnetism has been invaluable. I would also like to thank the head of the department, Professor Jari Hyttinen, PhD, for his guidance, especially during the initial stages. His contribution, together with that of Päivi Laarne, PhD, was inspirational for my investigations into the field of modelling.

I would also like to thank Docent Ville Jäntti, MD, for his guidance in planning the experimental EEG measurements. I also gratefully acknowledge the help of Pasi Kauppinen, PhD, and Riina Meriläinen-Juurikka, BEng, for setting up the multichannel EEG equipment for the measurements. I am also indebted to all my colleagues at Ragnar Granit Institute and especially all the volunteers who so kindly gave their time for the lengthy measurement sessions.

I wish to thank Sylvain Baillet, PhD, (Pierre & Marie Curie University, France), Geertjan Huiskamp, PhD, (University Medical Center Utrecht, The Netherlands) and Bart Vanrumste, Dr Ir, (Katholieke Universiteit Leuven, Belgium) for their constructive criticism and advice as examiners of this thesis. I also thank Alan Thompson, MPhil, for carefully revising the English of my thesis.

The financial support of The Graduate School of Tampere University of Technology, The Academy of Finland, The Finnish Cultural Foundation, The Wihuri Foundation and The Ragnar Granit Foundation is gratefully acknowledged.

I would also like to thank my parents and sister for all their support. Finally, my heartfelt gratitude goes to my husband Juho. He not only helped me strike a balance between work and leisure when I most needed it, but also as my colleague, contributed to my research.

Tampere, May 2008

Outi Vaarma

# TABLE OF CONTENTS

## LIST OF ORIGINAL PUBLICATIONS

This thesis is based on the following publications, referred to in the text by Roman numerals.

I. **Ryynänen O**, Hyttinen J, Laarne P, and Malmivuo J. Effect of electrode density and measurement noise on the spatial resolution of cortical potential distribution. *IEEE Transactions on Biomedical Engineering*, vol. 51, no. 9, pp. 1547-1554, 2004.

II. **Ryynänen O**, Hyttinen J, Laarne P, and Malmivuo J. Effect of measurement noise on the spatial resolution of EEG. *Biomedizinische Technik*, vol. 48, Supplement 2, pp. 94-97, 2004.

III. **Ryynänen O**, Hyttinen J and Malmivuo J. Effect of measurement noise and electrode density on the spatial resolution of cortical potential distribution with different resistivity values for the skull. *IEEE Transactions on Biomedical Engineering,* vol. 53, no. 9, pp. 1851-1858, 2006.

IV. Väisänen J, **Väisänen O**, Hyttinen J, and Malmivuo J. New Method for Analysing Sensitivity Distributions of Electroencephalography Measurements. *Medical & Biological Engineering & Computing*, vol. 46, no. 2, pp. 101-108, 2008.

V. **Ryynänen O**, Väisänen J, Hyttinen J, and Malmivuo J. Effect of source depth on the specificity of bipolar EEG measurements. In the *Proceedings of the 28th Annual International Conference of the IEEE Engineering in Medicine and Biology Society*, New York City, USA, 30.8.-3.9.2006 pp. 1110-1113.

VI. **Väisänen O** and Malmivuo J. Improving the SNR of EEG generated by deep sources with multielectrode leads. *Journal of Physiology - Paris*, submitted.

VII. **Väisänen O** and Malmivuo J. Improved Detection of Deep Sources with Weighted Multielectrode EEG Leads. In the *Proceedings of the 29th Annual International Conference of the IEEE Engineering in Medicine and Biology Society*, Lyon, France, 23.-26.8.2007 pp. 5194-5197.

---

Outi Ryynänen is the maiden name of Outi Väisänen

## AUTHOR'S CONTRIBUTION

Publications I – III concern the spatial resolution of cortical potential distribution. Professor Jari Hyttinen originally presented the idea of studying the effect of electrode number on the accuracy of the estimation of the cortical potential distributions. The author has otherwise designed the studies, implemented the method (excluding the programming of the numerical method) and prepared the results. The author has also written the papers, while receiving comments from the co-authors.

As co-author of Publication IV, the author has been involved in designing the new parameter also for the purposes of Publications V-VII. The author has also participated in designing the experimental measurements. The methods were implemented and the results were prepared by Juho Väisänen. The author also participated in the writing of the manuscript. In Publication V, the author implemented the methods, prepared the results and wrote the paper.

Publications VI and VII concern the development of the multielectrode lead method. The original idea of modifying the lead field with multichannel EEG to be optimal for deep sources was proposed by Professor Jaakko Malmivuo. The author has designed the studies, implemented the methods including the experimental measurements and prepared the results. The work was conducted under the supervision of the co-author. The author has also written the papers, while receiving comments from the co-author.

# LIST OF ABBREVIATIONS

| | |
|---|---|
| AC | alternating current |
| BAEP | brainstem auditory evoked potential |
| BEM | boundary element method |
| CIT | cortical imaging technique |
| CSF | cerebrospinal fluid |
| CT | computed tomography |
| DC | direct current |
| ECG | electrocardiography |
| ECoG | electrocorticography |
| EEG | electroencephalography |
| EIT | electrical impedance tomography |
| EMG | electromyography |
| EOG | electro-oculography |
| EP | evoked potential |
| FDM | finite difference method |
| FEM | finite element method |
| fMRI | functional magnetic resonance imaging |
| GWN | Gaussian white noise |
| HSV | half-sensitivity volume |
| LCMV | linearly constrained minimum variance |
| LORETA | low-resolution brain electromagnetic tomography |
| MEG | magnetoencephalography |
| MR | magnetic resonance |
| MUSIC | multiple signal classification |
| NL | relative noise level |
| PET | positron emission tomography |
| RBV | reconstructable basis vector |
| RMS | root mean square |
| ROI | region of interest |
| ROISR | region of interest sensitivity ratio |
| SEP | somatosensory evoked potential |
| SNR | signal-to-noise ratio |
| SPECT | single proton emission computed tomography |
| SVD | singular value decomposition |
| TSVD | truncated singular value decomposition |
| VEP | visual evoked potential |

# LIST OF SYMBOLS

| | |
|---|---|
| $\mathbf{A}$ | forward transfer matrix |
| $\mathbf{A}^+$ | pseudoinverse of matrix **A** |
| $\mathbf{b}$ | vector of EEG potentials |
| $\mathbf{c}_L$ | lead vector |
| $\mathbf{e}$ | measurement error vector |
| $I_r$ | reciprocal current |
| $\mathbf{J}^i$ | impressed current density |
| $\mathbf{J}_L$ | lead field current density |
| $n(t)$ | noise signal |
| $K(x_C,x_S)$ | kernel |
| $\mathbf{p}$ | source dipole |
| $s(t)$ | desired signal |
| $S_C$ | cortical surface |
| $S_S$ | scalp surface |
| $t$ | time |
| $\mathbf{u}_i$ | left singular vector |
| $\mathbf{v}_i$ | right singular vector |
| $\mathbf{u}_i^T\mathbf{b}$ | Fourier coefficient of **b** |
| $\mathbf{U}$ | left singular matrix |
| $\mathbf{v}_i^T\mathbf{x}$ | Fourier coefficient of **x** |
| $\mathbf{V}$ | right singular matrix |
| $V$ | volume |
| $V_L$ | measured potential |
| $w_i$ | weight of unipolar lead |
| $\mathbf{x}$ | source vector |
| $\mathbf{x}^+$ | least-squares solution |
| $x_C$ | location on the cortical surface |
| $x_S$ | location on the scalp surface |
| $x(t)$ | noise-contaminated signal |
| $\sigma$ | conductivity |
| $\sigma_i$ | singular value |
| $\mathbf{\Sigma}$ | singular value matrix |
| $\tau$ | error level |
| $\phi_S(x_S)$ | scalp surface potential |
| $\phi_C(x_C)$ | cortical surface potential |
| $\phi$ | electric potential |

# 1 INTRODUCTION

Electroencephalography (EEG) is a standard method in neurophysiology to study the function of the brain. Both spontaneous activity and evoked potentials (EP) can be measured with electrodes attached to the surface of the scalp. EEG has a wide range of clinical applications ranging from diagnosis of epilepsy and brain tumours to the analysis of sleep and the depth of anaesthesia. Measured evoked potentials, on the other hand, can be used in diagnosis of central nervous system diseases and in studies concerning the cognitive processes. (Nunez and Srinivasan 2006)

In addition to EEG, there are also other non-invasive techniques that can be used to monitor brain function. These include magnetoencephalography (MEG), functional magnetic resonance imaging (fMRI), positron emission tomography (PET) and single photon emission computed tomography (SPECT) (Gevins *et al.* 1990; Wikswo *et al.* 1993; Michel *et al.* 2004). EEG and MEG measure the electric and magnetic field, respectively, generated by the electrical activity of the brain, while fMRI, PET and SPECT measure the hemodynamic response (Shibasaki 2008). These methods differ in their temporal and spatial properties. The temporal resolution below the millisecond scale of EEG and MEG is superior to the other imaging modalities, whereas the spatial resolution of fMRI and PET is superior to that of conventional EEG and MEG.

It has been widely acknowledged that the spatial resolution of the traditional 10-20 – electrode system is not sufficient for modern brain research (Gevins *et al.* 1995; Gevins *et al.* 1999; Babiloni *et al.* 2001b; Michel *et al.* 2004). If the spatial resolution is poor, localization of the complex distribution of the electrical activation is difficult. Accurate localization is important for studying the fine topography related, for example, to higher order cognitive brain functions and seizure onsets as well as in planning tumour and epilepsy surgery. (Pohlmeier *et al.* 1997; Wang and He 1998; Gevins *et al.* 1999)

The spatial resolution of EEG is affected by blurring caused by volume conductor effects, the largest being the effect of the low conducting skull. A volume conductor model of the head can be constructed to study the effects of different tissues on the volume conduction. The most important characteristics of a head model are its geometrical shape and the resistivities assigned to different tissues. For a long time it was assumed that the resistivity of the skull is 80 times that of scalp and brain (Rush and Driscoll 1968, 1969),

but during the last decade it has been shown that this value is greatly overestimated (Oostendorp *et al.* 2000; Akhtari *et al.* 2002; Hoekema *et al.* 2003).

The spatial resolution of EEG can be improved by first increasing the number of measurement electrodes, and secondly, by applying a spatial enhancement method to reduce the effect of blurring. The multichannel EEG is nowadays convenient to apply because of the improvements in EEG amplifier technology and computerized signal processing methods. The Laplacian derivation (Hjorth 1975) was the first of the spatial enhancement methods to be introduced. It is a fairly simple method, which does not necessarily require the construction of a volume conductor model. Another possibility is to improve the spatial resolution by solving the inverse cortical source distribution. These methods are called source imaging methods and they require the construction of a volume conductor model. The spatial resolution is improved because the effect of the low conducting skull is taken into account. Examples of such methods are the cortical imaging technique (Kearfott *et al.* 1991; Sidman *et al.* 1992; Babiloni *et al.* 1997b; Wang and He 1998; Zhang *et al.* 2006a) and the deblurring method (Gevins *et al.* 1991; Le and Gevins 1993; Gevins *et al.* 1994; Gevins *et al.* 1999).

Most of the EEG signal measured from the scalp surface with two-electrode EEG leads is generated by cortical activity. When evoked potentials generated at deeper structures are measured, a typical means to improve the signal-to-noise ratio (SNR) is to average a large number, even thousands, of epochs. Beamformer methods have also been introduced to enhance the signals generated at different depths within the brain. Beamformers act as spatial filters. Beamformers are usually applied to source localization, but their basis is in passing the signals generated in the target region within the brain (Van Veen *et al.* 1997; Ward *et al.* 1999). Application of a large number of electrodes provides a means for optimizing the properties of the spatial filters.

An illustrative and simple way to study the sensitivity of different measurement leads is provided by the reciprocity and lead field theorems (Malmivuo and Plonsey 1995). The lead field analysis reveals that the sensitivity of two-electrode EEG leads is concentrated on the cortex (Malmivuo *et al.* 1997). The number of electrodes in both terminals of the lead can be increased to modify the sensitivity distributions. This method was introduced by McFee and Johnston (1954a), who modified electrocardiography (ECG) leads. With such multielectrode leads, it is possible to optimize the sensitivity distribution to be specific to sources at the target region, even those located deep within the brain.

# 2 OBJECTIVES OF THE STUDY

This thesis concentrates on two main topics, both of which show potential to benefit from the application of multichannel EEG. These two applications represent contrasting approaches to the application of a large number of electrodes on the surface of the scalp; in the first of these the focus is on cortical sources, whereas in the second, it is on the deep EEG sources.

*The first main topic* is devoted to studying the spatial resolution of cortical potential distribution. The purpose is to theoretically define, independent of the underlying source pattern, how many electrodes are needed to obtain the highest possible spatial resolution of the inverse cortical potential distribution. The effect of measurement noise plays the most important role in defining a sufficient number of electrodes. The effect of the widely debated resistivity of the skull was also studied. In detail, the objectives of this first topic are as follows:

- to study the effect of EEG electrode density on the spatial resolution of cortical potential distribution in the presence of measurement noise [I - III]
- to study the effect of skull resistivity on the spatial resolution of cortical potential distribution [III]

*The second main topic* concerns the development of new measurement leads to improve the SNR of EEG signals generated deep in the brain. For this purpose weighted multielectrode leads consisting of a large number of measurement electrodes were developed. The method is based on modifying the sensitivity distribution with the aid of the lead field theory. New parameters to describe the specificity of measurement sensitivity were also derived. In detail, the objectives of the second topic are as follows:

- to study the specificity of different EEG leads to detect signals generated at different depths within the brain [IV - V]
- to develop weighted multielectrode EEG leads to improve the SNR of EEG generated by sources located deep in the brain [VI - VII]

# 3 REVIEW OF THE LITERATURE AND THEORETICAL BACKGROUND

## 3.1 Electroencephalography (EEG)

### *3.1.1 Properties of EEG*

The first report on the measurement of the electrical activity of the brain was written in 1875 by British physician Richard Caton (1875), who measured the exposed brains of experimental animals. The first human EEG measurement was made by German neuropsychiatrist Hans Berger in 1924. One of the subjects reported in his first paper on human EEG (Berger 1929) was the existence of alpha rhythm. During the 1930s he published several other findings on human EEG related to different conditions. The first evoked potential studies were reported by George D. Dawson (1951), who stimulated electrically the ulnar nerve and measured the resulting evoked potentials. (Niedermeyer 2005b)

The typical clinically relevant frequency band of EEG is from 0.1 to 100 Hz. Sometimes a stricter band from 0.3 to 70 Hz is considered relevant. Amplitudes measured from the surface of the cortex can vary between 500 and 1500 $\mu V_{pp}$. The amplitudes are attenuated considerably when they are volume-conducted to the surface of the scalp. The amplitude of EEG measured from the scalp surface varies typically between 10 and 100 $\mu V_{pp}$. In adults the maximum amplitudes are typically below 50 $\mu V_{pp}$. The measured amplitudes are also affected by the location of the electrodes and by the interelectrode distance. (Niedermeyer 2005a)

EEG oscillations are not restricted to the above mentioned frequency band. So-called ultraslow EEG activity has a frequency band from DC to 0.3 Hz. EEG oscillations with higher frequencies than 100 Hz can also be measured. Curio (2005) refers to the high-frequency EEG oscillations between 400 and 1000 Hz by the term “ultrafast EEG”. Ultrafast EEG includes, for example, so-called $\sigma$-bursts which overlap the early somatosensory evoked potential (SEP) components. These bursts have generators both deep in the brain and on the cortex and they have a frequency around 600 Hz. The brainstem auditory evoked potentials (BAEP) are also an example of high-frequency

oscillations (Nuwer *et al.* 1994). The high-frequency oscillations have typically extremely low amplitudes.

EEG is characterised by good temporal resolution on a sub-millisecond scale, but the spatial resolution of conventional EEG is poor. The spatial resolution is affected by blurring, which occurs as the EEG signals are volume-conducted through the different tissues of the head. The spatial resolution of EEG can be improved by increasing the number of measurement electrodes and by applying a spatial enhancement method to reduce the effect of blurring.

### *3.1.2 Genesis of EEG signals*

EEG recorded from the surface of the scalp is mainly generated by the synchronous activity of populations of neurons on the cerebral cortex. The main generators of EEG are the postsynaptic potentials in the dendrites of large pyramidal neurons. These neurons are highly interconnected and approximately 85 % percent of all cortical neurons are these pyramidal cells oriented parallel to each other and perpendicular to the local cortical surface (Nunez and Srinivasan 2006). As several neurons activate synchronously through superposition, they generate such a dipole moment that results in a measurable potential difference on the surface of the scalp. According to Nunez and Srinivasan (2006) approximately 6 $cm^2$ of the cortical gyri tissue needs to activate synchronously to produce such measurable potentials at the scalp surface that can be detected without averaging. (Lopes da Silva and Van Rotterdam 2005; Nunez and Srinivasan 2006)

Evoked potentials are generated as a response to given stimuli. The stimuli can be sensory, motor, or cognitive. The evoked responses measured from the surface of the scalp have such a low signal level that averaging, for example, is needed to reduce the effect of noise. Evoked potentials generated in the brainstem can also generate measurable potentials on the surface of the scalp. These have extremely low SNR, and thus, averaging of even thousands of epochs is needed to reduce the effect of noise. An example of such EPs is the BAEPs, which are generated in the eighth cranial nerve, pons and midbrain. Three different kinds of sources have been suggested for generating these potentials measured on the scalp surface: (1) compound action potentials, (2) postsynaptic potentials and (3) changes caused in the current flow due to changes in volume conductor. The action potentials of myelinated fibres have a longer duration than those of unmyelinated fibres and thus they are able to produce very low measurable potentials on the surface of the scalp. (Scherg and von Cramon 1985; Nuwer *et al.* 1994; Chiappa and Hill 1997; Celesia and Brigell 2005; Nunez and Srinivasan 2006)

### *3.1.3 EEG electrode systems*

EEG has been traditionally measured using the standard international 10-20 electrode system developed in the 1950s (Jasper 1958). This system is still widely applied in clinical practice. The system includes 21 electrode locations positioned according to four reference points: the inion, nasion, and left and right preauricular points. The electrodes are placed at 10 % and 20 % intervals according to the reference points. In recent decades the development in amplifier technology has enabled the application of even hundreds of

electrodes to measure EEG. The 10-20 system was first extended to the 10-10 system, which is also called the 10 % system (American Electroencephalographic Society guidelines 1991). It is rather common in EEG studies to apply 64 electrodes, whose locations can be found from the 10-10 system. For nearly two decades, electrode systems consisting of over 100 electrodes have been studied (Gevins *et al.* 1990). These multichannel electrode arrays have been used especially for research purposes. Oostenveld and Praamstra (2001) suggested a 10-5 electrode system that includes up to 345 electrode locations and their nomenclature.

Formerly, EEG measurements were conducted by placing the electrodes individually on the surface of the scalp. Nowadays EEG measurements are usually made with electrode caps. Electrode cap manufacturers provide caps with up to 256 electrodes (Electrical Geodesics, Inc.; Electrocap International Inc; Neuroscan Quik-Caps). Electrode cap manufacturers have implemented the 10-20 and 64 electrodes of 10-10 system into the caps (Electrocap International Inc; Neuroscan Quik-Caps). Depending on the manufacturer, in the 128 and 256 channel caps the electrodes are placed as equidistantly as possible or part of the electrodes are placed according to 10-10 system locations. The need for precise electrode locations such as in the 10-20 system is nowadays unnecessary since the electrode locations can be registered either with digitizers (Polhemus) or with photogrammetric systems (Russell *et al.* 2005).

An interesting characteristic of different electrode systems, especially in studies concerning the spatial resolution, is the average interelectrode distance. Gevins *et al.* (1994) have approximated that these values for the typical adult head are 6 cm in a standard 10-20 system, 3.3 cm with 64 electrodes and 2.25 cm with 128 electrodes. The interelectrode distance of the 256 electrode system is approximated to be 1.6 cm (Gevins *et al.* 1991). Multichannel EEG caps are illustrated in Figure 3.1, where (a) is a 124-channel and (b) a 256-channel Neuroscan EEG cap.

The average interelectrode distance also depends on the layout of the cap. The Geodesic caps (Electrical Geodesics, Inc.) cover the scalp surface more comprehensively than, for example, the 10-20 or 10-10 systems or the Neuroscan caps (Srinivasan *et al.* 1998). It is typical of the Geodesics' caps that the electrodes are also placed over the neck and facial area. Thus the average interelectrode distances in Geodesic caps are longer, being 38 mm, 28 – 30 mm and 20 mm for 64, 128 and 256 electrodes, respectively (Tucker 1993).

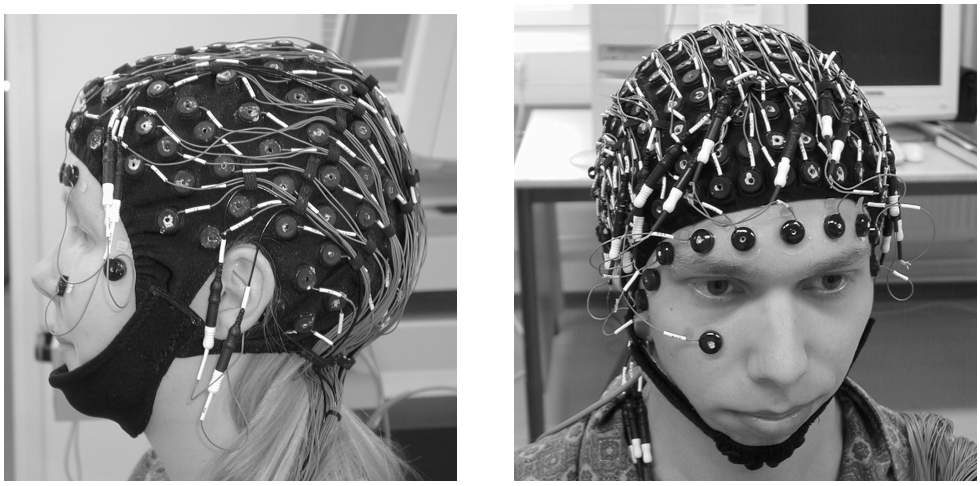

(a) (b)

Figure 3.1. Multichannel EEG caps. a) a 124-channel Neuroscan EEG-cap and b) a 256-channel Neuroscan EEG-cap.

### *3.1.4 Noise in EEG measurements*

Because of the very low signal amplitude, noise has a notable effect on the quality of the measured EEG signals. Depending on the type of EEG measurement, the noise in EEG can be separated into different components; noise generated within the brain, other bioelectric noise components, electrode noise, noise coupled from the environment and noise generated in the measurement device. Scheer *et al.* (2006) studied separately the effect of biological noise, amplifier noise and electrode interface noise on signal quality. They concluded that the highest of the biological noise components is the background activity generated at the cortex. Also, for low frequencies below 100 Hz, the noise is mainly composed of activity generated at the cortex. At high frequencies, on the other hand, the interface noise and amplifier noise mainly affect the SNR.

*NOISE GENERATED IN THE BRAIN*

In evoked potential measurements, the true signal is only that part of EEG that is generated as a response to a given stimulus. All the other activity generated within the brain is considered as noise. The dynamics of the background EEG, which mostly consists of the cortical activity, can range between extremes of coherent and incoherent behaviour (Nunez *et al.* 1999). The estimation of the properties of the background noise is considered, for example, in so-called minimum likelihood dipole localization methods (Lütkenhöner 1998a, 1998b) where an estimate of the covariance matrix of the noise is applied to improve the source localization accuracy. In some studies, randomly distributed dipoles within the brain have been applied to simulate the background EEG activity (de Munck *et al.* 1992; Lütkenhöner 1998a, 1998b). Studies have also been conducted on the effects of different factors affecting the EEG coherence (Nunez *et al.* 1997; Nunez *et al.* 1999; Srinivasan *et al.* 2007).

The correlation of background EEG signals depends on many factors including the type of activity and the frequency band. The correlation of the signals measured on the surface of

the scalp results partly from the volume conductor effects. Nunez *et al.* (1997, 1999) and Srinivasan *et al.* (2007) have extensively studied the effect of volume conduction on the correlation. When they simulated the background EEG with uncorrelated radial cortical dipoles, it was observed that with electrode distances shorter than 10 cm, the scalp EEG is correlated. The shorter the distance, the higher is the correlation. Nunez *et al.* (1999) and Srinivasan *et al.* (2007) also studied the coherence of experimental EEG measurements conducted during different functional brain states. For example, during alpha activity high coherence is observed in the alpha frequency band over long electrode distances. The high coherence results both from volume conductor effects and genuine cortical source coherence. Srinivasan *et al.* (2007) showed that for a higher frequency band (40-50Hz), the coherence is similar to that obtained in the simulation conducted with uncorrelated sources. Thus they concluded that cortical sources generating spontaneous EEG in a frequency band 40-50Hz are apparently uncorrelated.

*OTHER BIOELECTRIC NOISE COMPONENTS*

The non-cerebral bioelectric activity may also produce noise components in the measured signal. Electro-oculogram (EOG) is generated by eye movement and blinking. Depending on the locations of the electrodes and the direction of the eye movement, the EOG artefact may have substantially higher amplitude than the EEG activity. The frequency of EOG is usually below 50 Hz (Olson 1998). Electrical activity of the heart can also generate an artefact in EEG signals. In some cases it is beneficial to separately measure the EOG and ECG signals, so that they can be adopted for artefact rejection or noise cancellation (Sörnmo and Laguna 2005). Electromyography (EMG) signals generated by muscle activity produce the most severe bioelectric noise component because of its frequency spectrum. It is also impossible to measure EMG activity independently of the EEG for noise cancellation. Most of the EMG spectral power measured with surface electrodes is below 400-500Hz (Sörnmo and Laguna 2005).

*ELECTRODE INTERFACE NOISE*

A great portion of noise in surface biopotential measurement is generated by electrodes (Fernandez and Pallas-Areny 2000; Huigen *et al.* 2002). The noise generated at the electrodes comprises two components: the component generated at the metal-electrolyte interface and the component generated at the electrolyte-skin interface. The former has such low magnitude ($< 1\mu V_{rms}$) that it cannot be separated from instrumentation noise (Huigen *et al.* 2002). The latter component, on the other hand, can be of the order of $1 – 20\ \mu V_{rms}$ (Fernandez and Pallas-Areny 2000; Huigen *et al.* 2002) and thus generates a notable noise component in the recordings. The electrode noise decreases monotonically as a function of frequency and is notably high at low frequencies below 30 Hz. At around 50 Hz the electrode noise decreases to the level of amplifier noise (Huigen *et al.* 2002). The magnitude of electrode noise depends, for example, on the area of the electrode, the paste material, preparation of the skin and the time spent after preparation of the electrode sites. Huigen *et al.* (2002) have shown that of the typically applied electrode materials, Ag-AgCl electrodes stabilize almost immediately after the application, whereas with steel electrodes, stabilization might take up to three hours.

*NOISE COUPLED FROM THE ENVIRONMENT*

The AC devices in the recording environment and the power lines generate a 50 Hz noise component in the EEG data. This noise introduced by other devices can be either magnetically or capacitively coupled to the EEG measurement. The coupling occurs especially through the measurement leads (Ferree *et al.* 2001b). The higher the electrode impedances are, and especially the higher their imbalance is, the larger is the amplitude of capacitively coupled noise (Metting van Rijn *et al.* 1990; Neuman 1998; Ferree *et al.* 2001b; Kamp *et al.* 2005). Thus it is of great importance to minimise the electrode impedances and their imbalance in the measurements. The magnitude of magnetic coupling depends on the areas of the loops formed, for example, by the measurement leads. The effect of magnetic coupling can be reduced by twisting the measurement leads (Ferree *et al.* 2001b).

*NOISE GENERATED IN THE MEASUREMENT DEVICE*

In electronic amplifiers there always exists white and pink noise. White noise has a constant power spectral density over the frequency band, whereas the power spectral density of pink noise is inversely proportional to frequency. This noise depends on factors such as the design of the amplifier and the measurement bandwidth. Typical electronic noise levels are 1 – 2 $\mu V_{pp}$ and 4 $\mu V_{pp}$ for 100 Hz and 3 kHz bandwidths, respectively. (Kamp *et al.* 2005)

### *3.1.5 SNR Improvement of EEG measurements*

In every EEG measurement some noise will always persist despite all efforts to reduce its components. Thus different artefact rejection and noise cancellation methods have been developed to reduce the noise and to improve the SNR. When the frequency spectrum of the noise signals is different from that of the EEG signal, linear filtering can be applied to cancel the noise. The problem with EEG is that most of the noise signals have a similar frequency spectrum to EEG. (Sörnmo and Laguna 2005)

In EP measurements the most typical approach is to average several responses to improve the SNR. Depending on the amplitude of the signal, the number of epochs that needs to be averaged can vary from a few tens up to several thousands. In the time averaging of evoked potentials it is assumed that the measured stochastic signal *x(t)* is the sum of actual signal *s(t)* and additive stochastic noise *n(t)*. If the noise samples are uncorrelated, the amplitude SNR increases proportionally to square root of the number of averaged epochs. This additive model might only be valid under anaesthesia and for short latency evoked potentials. For longer latencies, the assumption of additive noise has been shown to be insufficient and more complex models are needed. (Lopes da Silva 2005)

Depending on the statistical properties of the desired signal and the noise signal, multichannel EEG can be applied to improve the SNR of measured EEG compared to sparser electrode systems. A simple example is the case where the desired signal is correlated over several electrodes in a multichannel measurement whereas the noise is uncorrelated. In such as case, by spatially averaging signals measured with adjacent electrodes, the multichannel EEG measurement can be downsampled, for example, to a

10-20 system measurement. In the downsampled multichannel measurement the SNR is higher than if the measurements had originally been conducted with the 10-20 system.

## 3.2 EEG Inverse problems

### *3.2.1 Definition of an EEG inverse problem*

To understand the relationship between EEG sources and measured signals, the forward or inverse problems of EEG can be studied. For this purpose a model of a source and of a volume conductor is needed as illustrated in Figure 3.2. The inverse problem is the one that is of clinical interest; the purpose is to solve the sources based on the EEG data and the volume conductor model. The inverse problem does not have a unique solution, but an infinite number of intracranial source configurations can generate similar scalp potential distribution. Thus constraints must be placed on the source model. These constraints can include the number, type and location of the sources (Malmivuo and Plonsey 1995; Lagerlund and Worrell 2005). The selection of the constraints is a crucial step because an incorrect selection may lead to a solution that does not give any neurophysiologically relevant information about the generators (Michel *et al.* 2004).

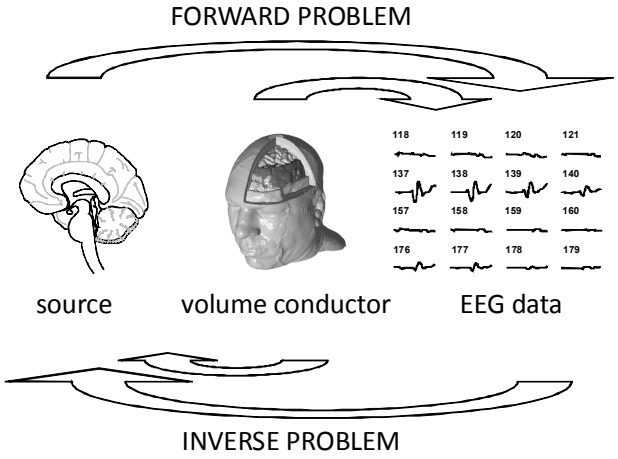


Figure 3.2. Definition of the forward and inverse problem.

There are various ways to categorise EEG inverse problems. In this thesis the EEG inverse problems are divided into two groups in terms of the properties of the applied source model. In the first group of methods, the source is modelled as single or multiple dipoles. Here these methods are called discrete source localization methods. The second group of methods apply a distributed source model and here these methods are called source imaging methods. (Babiloni *et al.* 2003; Michel *et al.* 2004; Lagerlund and Worrell 2005)

### *3.2.2 Discrete source localization methods*

The nature of the postsynaptic potentials generating the EEG gives a physical explanation for the use of the dipolar source model. At the level of the synapse, there exists either a local source or sink, which is balanced either by a distributed sink or source along the cell, respectively. The distance between the cortical surface and the scalp is large enough for

the potentials measured at the surface of the scalp to behave as if they were generated by a dipolar source. (Lopes da Silva and Van Rotterdam 2005; Nunez and Srinivasan 2006) When several parallel neurons activate synchronously, the local dipoles form a dipole layer. The dipole source model is mainly suited to problems when the source is relatively small. These kinds of sources are, for example, those located in deep structures such as brainstem or thalamus. If the dipole localization is applied to more widespread sources, it is important to recognise that the estimated dipole source is an equivalent source: its strength is a sum of all individual dipolar source components and its location is at the centre of the mass of the active region. (Lagerlund and Worrell 2005)

The major limitation of dipole localization is that the number of dipolar sources has to be decided before solving the inverse problem. Different dipole localization algorithms aim to solve the location, orientation and strength of a single or multiple dipoles on the basis of spatial or spatio-temporal data (Michel *et al.* 2004; Lagerlund and Worrell 2005). The first spatio-temporal dipole model was introduced by Scherg and von Cramon (1985, 1986). Another widely applied method is the multiple signal classification (MUSIC) developed by Mosher *et al.* (1992) and its improved versions (Mosher and Leahy 1998, 1999). The MUSIC methods produce an image-like solution, but here it is considered as a discrete source localization method, since an estimate of the number of dipolar sources is needed in this signal subspace method.

### *3.2.3 Source imaging methods*

The major advantage of EEG source imaging methods over source localization methods is that no assumption about the number of sources is needed beforehand. In the first group of source imaging methods, the source space consists of the whole brain volume. These methods include, for example, minimum norm solution (Hämäläinen and Ilmoniemi 1994), weighted minimum norm solution, low-resolution brain electromagnetic tomography (LORETA) (Pascual-Marqui *et al.* 1994), beamformer approaches (van Drongelen *et al.* 1996; Van Veen *et al.* 1997) and Bayesian approaches. (Michel *et al.* 2004)

*BEAMFORMERS*

Beamformers are spatial filters originally used in radar and sonar applications (Van Veen and Buckley 1988). The purpose in the spatial filtering methods is to enhance the signal generated at the target region while suppressing the noise signals originated at other locations (van Drongelen *et al.* 1996; Van Veen *et al.* 1997). Due to the nature of spatial filters, in addition to source imaging applications, they can be applied to improve the SNR of signals generated at the target region within the brain. Ward *et al.* (1999) applied beamformers to enhance deep epileptiform activity. The most common of the spatial filtering methods is a so-called linearly constrained minimum variance (LCMV) method, but also other methods to optimize the beamformer output have been presented (Van Veen and Buckley 1988). When the beamformers are applied to solve the inverse problem, the whole brain volume is scanned and the neural activity index is calculated, which describes the activity at a certain location (Van Veen *et al.* 1997). The sources are assumed to be located at the locations of highest activity index.

*CORTICAL IMAGING METHODS*

The second group of source imaging methods are the so-called cortical imaging methods. In cortical imaging methods the purpose is to solve either the current density or potential distribution on the cortical surface or, to be more precise, on an imaginary layer, which is located immediately above the cortex. If this layer is defined as a closed layer, the solved source distribution presents all the activity which is generated within the closed surface (Yamashita 1982). An important characteristic of cortical imaging methods is their ability to reduce the effect of blurring, which happens when the signals are volume-conducted from the cortical surface through different tissues to the surface of the scalp. The cortical imaging methods are also called spatial enhancement, spatial deconvolution or spatial deblurring methods because they provide a much higher spatial resolution than the scalp potential distribution. The cortical imaging methods include the Laplacian methods (Hjorth 1975), the cortical imaging technique (CIT) (Kearfott *et al.* 1991) and the deblurring method (Gevins *et al.* 1990).

In source imaging methods the source is always an equivalent source. However, in contrast to dipole localization methods, the result of source imaging has a physiological relevance because it resembles the potential distribution that would be invasively measured from the cortical surface. Thus the non-invasively solved cortical potential distribution might provide equal information about the sources as the highly invasive electrocorticography (ECoG), which has been traditionally employed for identifying the location and extent of the epileptogenic brain tissue prior to surgical removal. (Zhang *et al.* 2003; Quesney and Niedermeyer 2005) At least the non-invasively solved cortical potential distribution can be applied for optimizing the locations for subdural grids (Gevins *et al.* 1999).

In some applications it may be useful to apply a source imaging method prior to source localization to approximate the complexity of the source distribution. The solved distribution may also help in deciding the appropriate number of dipolar sources to be solved. If the complexity of the distribution is too great, the dipole localization can be abandoned for not providing a realistic estimate of the EEG sources. (Nunez and Srinivasan 2006)

Many of the methods that have been applied to solving the cortical potential distribution as a solution of an inverse problem have been modified from methods that were developed to solve the epicardial potential distribution in the case of ECG. These two methods have the same theoretical basis. In the case of EEG, the volume conductor consists of the volume between the closed cortical surface and the closed scalp surface. In the case of ECG, the volume conductor consists of the volume between the closed epicardial surface and torso surface. The volume $V$ can be either homogeneous or inhomogeneous. An example of the volume conductor is illustrated in Figure 3.3, where the volume $V$ is bounded by two closed surfaces $S_S$ and $S_C$. The volume $V$ is so selected that it does not include any sources. In the case of EEG, the inner surface $S_C$ is defined above the cortical surface and, thus, it encloses all the sources within the brain.

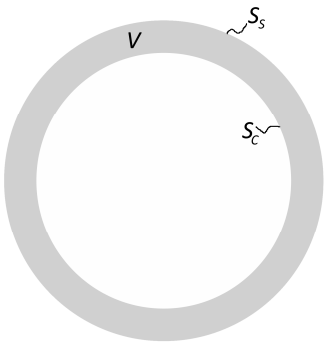


Figure 3.3 Volume conductor model in cortical potential imaging. Volume $V$ is surrounded by two closed surfaces $S_C$ and $S_S$. The volume $V$ can be inhomogeneous and anisotropic.

Barr *et al.* (1977) were the first to describe a method where torso surface potentials were calculated on the basis of the epicardial potentials. In their method, the volume conductor was homogeneous between the two closed surfaces. They applied Green's second identity to the volume and derived the equations for relating the two surface potentials. The relationship between source potential distribution and the field distribution can be given as (Yamashita 1982; Yamashita and Takahashi 1984):

$$\phi_S(x_S) = \int_{S_C} K(x_C, x_S)\phi_C(x_C)\,dx_C, \qquad x_S \in S_S \text{ and } x_C \in S_C \tag{3.1}$$

where $\phi_S(x_S)$ are the scalp surface potentials, $\phi_C(x_C)$ are the cortical surface potentials, $S_C$ is the closed cortical surface, $S_S$ is the closed scalp surface. $K(x_C,x_S)$ is the kernel, also called Green's function, which is provided by the solution of the forward problem (Yamashita 1982). If the potential on the cortical surface is zero everywhere else, except at location $x_C$ where it has a magnitude of one, then $K(x_C,x_S)$ is the potential value at point $x_S$ (Greensite 2004). A great benefit in solving the cortical potential distribution from the scalp potential data is that the problem has theoretically a unique solution (Yamashita 1982). In practice, however, the accuracy is limited by the discrete sampling of the potentials on the surface and by the measurement noise.

### *3.2.4 Formulation of the EEG inverse problem*

The forward problem of EEG can be mathematically formulated as a set of linear equations:

$$\mathbf{Ax} = \mathbf{b} \tag{3.2}$$

where **A** is a forward transfer matrix containing the information on the source-field relationship, **x** is a vector containing information on the magnitude of the sources and **b** is a vector containing the potentials measured on the scalp surface. The forward transfer matrix **A** reflects the properties of the volume conductor. It is an $m$ x $n$ matrix, where $m$ is the number of electrodes and $n$ is the number of source components to be solved. The source imaging methods are underdetermined and thus $n >> m$.

In the case of inverse problems, the purpose is to solve **x** from Equation (3.2). Depending, for example, on the properties of the sources and the forward transfer matrix, there are different methods for solving the problem. One possibility is to solve the pseudoinverse $\mathbf{A}^+$ of matrix **A** with singular value decomposition (SVD). In singular value decomposition the matrix **A** is decomposed into a product of three matrices:

$$\mathbf{A} = \mathbf{U}\mathbf{\Sigma}\mathbf{V}^T = \sum_{i=1}^{m} \mathbf{u}_i \sigma_i \mathbf{v}_i^T \tag{3.3}$$

where **U** is an *m* x *m* orthogonal matrix, **V** is an *n* x *n* orthogonal matrix and $\mathbf{\Sigma}$ is an *m* x *n* diagonal matrix whose elements $\sigma_i$ are real and non-negative. The column vectors $\mathbf{v}_i$ are the orthonormal basis vectors of the source space and the columns $\mathbf{u}_i$ are the orthonormal basis vectors of the surface potential space. The singular values $\sigma_i$ are organized in non-descending order: $\sigma_1 \geq \sigma_2 \geq \ldots \geq \sigma_m \geq 0$ (Golub and Van Loan 1989).

SVD is also a practical means to study how ill-posed the problem in Equation (3.2) is. In discrete ill-posed problems there are two typical characteristics of the SVD (Hansen 1998). Firstly all the singular values $\sigma_i$ decay gradually towards zero. Secondly, the elements of the basis vectors $\mathbf{v}_i$ and $\mathbf{u}_i$ tend to have more sign changes as the index *i* increases. The matrix **A** in the discrete ill-posed problems is always highly ill-conditioned. The condition number of matrix **A** can be calculated to measure the sensitivity of the solution **x** to the perturbations in **b** or **A**. The condition number is defined as a ratio of the largest to smallest singular value. The higher the condition number, the more ill-conditioned the problem is.

With SVD the solution to the inverse problem can be calculated as:

$$\mathbf{x}^+ = \mathbf{A}^+\mathbf{b} = \sum_{i=1}^{m} \frac{\mathbf{u}_i^T \mathbf{b}}{\sigma_i} \mathbf{v}_i \tag{3.4}$$

Equation (3.4) indicates that for small singular values $\sigma_i$, the high-frequency components in **b** are amplified. Because of the ill-posed nature of the inverse problems, the solution needs to be regularized. One possibility to stabilize the solution is to replace the smallest singular values with zero. This method is called truncated singular value decomposition (TSVD). Another widely applied regularization method in EEG source imaging studies is the Tikhonov regularization method (He *et al.* 2002b; Zhang *et al.* 2003). Methods including the L-curve and discrepancy principle have been applied to select the regularization parameter in Tikhonov regularization or the truncation point in TSVD. (Hansen 1998)

### *3.2.5 Effect of noise in EEG inverse solutions*

The amount of noise in the EEG data affects the amount regularization that is needed to obtain stable inverse solutions. When TSVD is applied as a regularization method, the goal is to find the correct index *i*, from which point onward to truncate the singular values. If

the index is too small, some spatial information of the solution is lost because the high-frequency components are truncated. On the other hand, if the index is too large, the solution will be unstable and noisy as described above.

Dössel and colleagues applied a TSVD-based method to study the "nullspace of electrocardiography" (Dössel and Schneider 1997; Dössel *et al.* 1998; Schneider *et al.* 1998; Schneider 1999). They have applied the method, for example, to optimize the number and locations of the electrodes in ECG inverse problems. Their method investigates the extent to which the noise level of the measured data influences the optimization procedure (Dössel *et al.* 1998). Estimation of the measurement error plays an important role in the procedure.

The basis vectors $\mathbf{v}_i$ belonging to the nullspace of **A** cannot be reconstructed. The normal nullspace is spanned by the basis vectors $\mathbf{v}_i$ of the source space, with index $i > m$. If the measurement data **b** is contaminated by measurement errors including noise, there exists a set of basis vectors $\mathbf{v}_i$ which lead to a signal smaller than the measurement noise. These basis vectors belong to the extended nullspace of matrix **A**. The essential question, in terms of obtaining a stabilized inverse solution and also sufficient spatial resolution, is to choose a correct index $i < i_m$ from which point onward to truncated the singular values.

Dössel *et al.* (1998), Schneider *et al.* (1998) and Schneider (1999) have derived the definition for the extended nullspace. It consists of the basis vectors which lead to a signal smaller than the measurement noise. The rough estimate for the nullspace is that it starts with the index $i$ of the first normalized singular value $\sigma_i/\sigma_1$ that is smaller than the relative measurement error.

Hansen (1998) has also identified which SVD components can be recovered in the presence of errors. The errors in **b** and **A** are treated separately. If there are no errors in the system, the singular values $\sigma_i^{\text{exact}}$ of $\mathbf{A}^{\text{exact}}$ decay gradually towards zero. Also the Fourier coefficients $|(\mathbf{u}_i^{\text{exact}})^{\mathrm{T}}\mathbf{b}^{\text{exact}}|$ of **b** decay, on average, to zero. In the presence of errors, the behaviour of singular values and Fourier coefficients differ from the previous as follows: the singular values $\sigma_i$ decay until they tend to settle at an error level $\tau_A$ determined by errors in **A**. The Fourier coefficients $|\mathbf{u}_i^{\mathrm{T}}\mathbf{b}|$ also decay, on average, until they settle at an error level $\tau_B$ determined by the errors in **b**. These two error levels determine how much information about the exact underlying system can be extracted from the given system.

Measurement errors in **b** are typically larger than other types of error in **A** and **b**. In this situation the Fourier coefficients settle at $\tau_B$ for $i > i_B$ earlier than singular values settle at $\tau_A$ for $i > i_A$. Thus it is possible to recover only the first $i_B$ components of the solution. The remaining $m - i_B$ components are dominated by the errors. The Fourier coefficient of **x** consists of two components (Hansen 1998):

$$\mathbf{v}_i^T\mathbf{x} = \mathbf{v}_i^T\mathbf{x}^{exact} + \frac{\mathbf{u}_i^T\mathbf{e}}{\sigma_i} \tag{3.5}$$

At $i = i_B$ the two components on the right hand side are of approximately the same size (Hansen 1998).

Related to the previous examination, in (Skipa 2002) the equation for the "nullspace of electrocardiography" was derived in a slightly different way than it was in (Dössel *et al.* 1998; Schneider *et al.* 1998; Schneider 1999). Combining Equations (3.2) and (3.3) gives the relationship

$$\sigma_i\mathbf{v}_i^T\mathbf{x} = \mathbf{u}_i^T\mathbf{b} \tag{3.6}$$

The measurement data **b** can be considered to consist of the exact measurement data $\mathbf{b}^{exact}$ and the measurement error **e**. Substituting these in Equation (3.6) gives Equation (3.5). Now at the index *i*, where the truncation needs to be performed, the two components on the right hand side are approximately of equal value. In the derivation of (Skipa 2002) it is assumed that the error is negligible when the contribution of the first source basis vector is reconstructed:

$$\sigma_1\mathbf{v}_1^T\mathbf{x}^{exact} = \mathbf{u}_1^T\mathbf{b} \tag{3.7}$$

To derive the truncation point $i = i_B$ Equations (3.5) and (3.7) are compared

$$\frac{\left\|\mathbf{v}_i^T\mathbf{x}^{exact}\right\|}{\left\|\mathbf{v}_1^T\mathbf{x}^{exact}\right\|} \approx \frac{\left\|\frac{\mathbf{u}_i^T\mathbf{e}}{\sigma_i}\right\|}{\left\|\frac{\mathbf{u}_1^T\mathbf{b}}{\sigma_1}\right\|} \tag{3.8}$$

The relation in (3.8) depends on the Fourier coefficient $\mathbf{v}_i^T\mathbf{x}^{exact}$ of the source vector **x**. Because the analysis is made solely on the basis of the known forward transfer matrix **A**, these Fourier coefficients can only be approximated. In (Skipa 2002) it is assumed that all the source basis vectors are presented equally in the source distribution. This is probably the best approximation since the intensities cannot be known without knowledge of the source vector, which is the intended solution of the inverse problem. With this approximation, from (3.8) it can be derived that

$$\frac{\sigma_i}{\sigma_1} \approx \frac{\left\|\mathbf{u}_i^T\mathbf{e}\right\|}{\left\|\mathbf{u}_1^T\mathbf{b}\right\|} \approx \frac{\|\mathbf{e}\|}{\|\mathbf{b}\|} \tag{3.9}$$

This result is similar to the equation derived in (Dössel *et al.* 1998; Schneider *et al.* 1998; Schneider 1999) and gives a rough estimation for the maximal index *i* of the source basis vectors that can still be reconstructed. The relation $||\mathbf{e}||/||\mathbf{b}||$ in (3.9) is known as the relative noise level (NL). The same formula for the selection of the truncation parameter

has also been applied by Gencer and Williamson (1998), who studied the reconstruction of neural source with EEG, MEG and multimodal EEG/MEG. From Equation (3.9) it is apparent that when the relative noise level is high, only a small portion of the basis vectors can be reconstructed, all other SVD components being dominated by the measurement noise (Hansen 1998).

## 3.3 Volume conductor models

### *3.3.1 Properties of volume conductor models*

The most important characteristics of a head volume conductor model are its shape and the resistivities of different tissues (Malmivuo and Plonsey 1995; Laarne 2000; Nunez and Srinivasan 2006). Volume conductor models of a human body may be considered as quasi-static. This means that the currents behave at any instant as if they were stationary. The quasi-stationarity follows from the fact that, within the volume conductor, the propagation effects can be neglected. In addition, the capacitive and inductive effects can be neglected and the volume conductor can be considered purely resistive (Geselowitz 1963; Plonsey and Heppner 1967). The quasi-static assumption holds up to several kilohertz (Geselowitz 1963), within which range the frequency of EEG falls. The volume conductor can also be considered linear. With the above assumptions, the Laplace and Poisson equations are valid and they can be applied to solve the bioelectric field problems.

### *3.3.2 Geometry of the model*

One of the most commonly employed of the head volume conductor models is an inhomogeneous, three-dimensional model consisting of three concentric spheres describing the brain, skull and scalp (Rush and Driscoll 1969). In the Rush and Driscoll three-layer spherical head model, the radii of the spheres representing the scalp, skull and brain are 9.2 cm, 8.5 cm and 8.0 cm, respectively. The fit of a three-layer spherical head model to the real anatomy is illustrated in Figure 3.4. Spherical models, which also include a fourth layer representing the cerebrospinal fluid (CSF), have been widely studied (Cuffin 1990).

One step towards more accurate models is the eccentric shell models (Meijs and Peters 1987; Fender 1991) and ellipsoidal models (Cuffin 1990). However, none of these models can describe the head geometry accurately. This is why nowadays the trend is towards realistically shaped head models. Such models can be constructed individually for every head geometry and thus provide geometrically more accurate models. Realistically shaped models can be constructed, for example, from magnetic resonance (MR) images or computed tomography (CT) images. (Fender 1991; Huiskamp *et al.* 1999; Laarne 2000). With realistically shaped models it is possible to include many additional tissues and anatomical details into the models. These include, for example, tissue compartments like grey matter, white matter, cavities, eyes, blood, spinal cord, cerebellum, hard and soft bone of the skull, fat and internal air (Haueisen *et al.* 1997; Ramon *et al.* 2004; Ramon *et al.* 2006).

When a realistically shaped head model is applied, a numerical method is needed to solve the Laplace's or Poisson's equation. These numerical methods include boundary element method (BEM), finite element method (FEM) and finite different method (FDM). If the model is spherically symmetric, analytical methods can be applied instead of numerical methods.

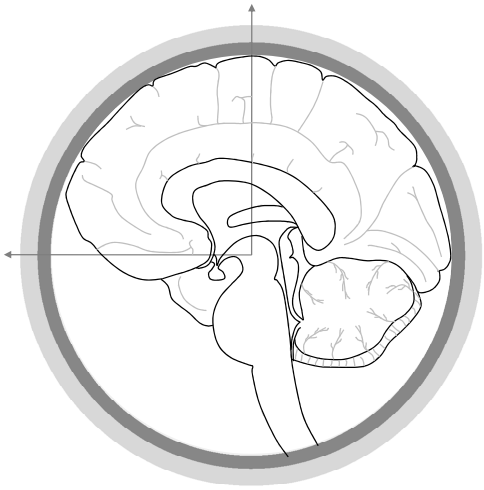

Figure 3.4. Sagittal view of a three-layer spherical head model and how it fits to the real anatomy.

The need for applying a realistically shaped head model has been widely discussed. Some researchers prefer the application of simple spherical models, while others prefer the application of realistically shaped head models. The major criticism of the latter head models concerns the selection of the correct resistivity values for different tissues. The effective resistance depends on both the tissue resistivity and thickness. Thus it has been claimed that the uncertainties in the conductivity are generally as critical as similar uncertainties in geometry (Nunez and Srinivasan 2006). Vanrumste *et al.* (2002) evaluated the effect of the head geometry on the dipole localization accuracy in the presence of noise. They concluded that as the effect of noise increases, the advantage of realistically shaped head models over the three-layer spherical head model is decreased. They concluded that when the noise level is below 0.1, the application of a realistically shaped head model significantly improves the dipole localization accuracy over the three-layer spherical head model.

The accuracy of the realistic geometry also depends on the type of images from which the models are constructed (Huiskamp *et al.* 1999; Wendel *et al.* 2008). The MR images are accurate in imaging the soft tissues, including the scalp and the boundary between the grey and white matter. On the other hand, the skull cannot be accurately imaged with MR scanners. The CT images, however, are specifically suited for imaging the skull. The radiation load of CT imaging severely restricts its application for model construction purposes. Different methods have also been developed to improve the segmentation of the skull layer from MR images. Dogdas *et al.* (2005) developed a segmentation method to define the skull from T1-weighted MR images. Their results showed that, for the upper portion of the head, the segmented skull from the MR images corresponded adequately to those segmented from CT images.

### *3.3.3 Electrical properties of the model*

In addition to the selection of the head geometry and tissue types included in the head model, the resistivity values assigned to different tissues affect the electric fields within the head. Defining the resistivity values for the tissues included in the model is not a straightforward task because the resistivity values are individual and vary with temperature and field frequency (Geddes and Baker 1967; Gabriel *et al.* 1996a; Gabriel *et al.* 1996b; Laarne 2000). There is considerable controversy in the literature over the values for different tissues. If the relative strengths of sources are the sole topic of interest, it is only necessary to model correctly the relative resistivities. (Oostendorp *et al.* 2000)

When assigning the resistivities to different tissues, the direction dependence, i.e., the anisotropy of the resistivity can be taken into account. However, most often the resistivities are considered isotropic, which means that the resistivity is similar in all the directions of the field and current flow. Some researchers consider the skull as having anisotropic conductivity. Usually an anisotropy ratio of 10 has been applied between the resistivities radial and tangential to the skull (de Munck 1988; Hallez *et al.* 2005; Wolters *et al.* 2006). In addition, the resistivity of the white matter is anisotropic because the myelin sheet decreases the conductivity perpendicular to the fibre orientation. Usually a ratio of 9 has been applied between the resistivities parallel and perpendicular to the fibre orientation in white matter (Nicholson 1965; Hallez *et al.* 2005; Wolters *et al.* 2006). Anisotropy of cerebral cortex with a ratio of two for the resistivity parallel and perpendicular to the fibre orientation has been reported (de Munck 1988).

### *3.3.4 Skull resistivity*

The relatively high value of the skull resistivity has the largest effect on the electric fields, and thus its properties are discussed separately in this section. For example, Nunez and Srinivasan (2006) have proposed that the application of correct skull resistivity is even more important than the application of realistic head geometry.

The structure of the skull varies over different lobes and the sutures also affect the resistivity. The skull is mainly composed of three different layers: the two outer layers are compact cortical bone and between these two layers is a spongy middle layer, the cancellous bone (Nunez and Srinivasan 2006). The resistivity of the cortical bone is much higher than the resistivity of the cancellous bone (Akhtari *et al.* 2000; Akhtari *et al.* 2002). Thus when the skull is considered as a homogeneous tissue, the resistivity in the tangential direction is lower than in the radial direction, which is the reason for considering the skull anisotropic (Law 1993; Nunez and Srinivasan 2006; Sadleir and Argibay 2007). However, the whole skull is not composed of this layered structure; at some points, the skull is mostly composed of compact cortical bone and at the suture lines, the skull resistivity is lower than at the solid areas (Law 1993). If the skull were composed only of this three layered bone, there would be a better case for applying constant thickness for the skull layer. At those areas where the skull is composed of three layers, it has been shown that there is an inverse relationship between skull thickness and resistivity because the thicker skull regions occur mainly as a result of increased thickness of the middle layer of cancellous bone (Law 1993). Thus the attempt to correct the

volume conductor model using only the real skull thickness information while ignoring the different resistivities of the layers, may reduce the model accuracy (Nunez and Srinivasan 2006). Another possibility is to model the three different layers of the skull as separate homogeneous isotropic layers (Haueisen *et al.* 1997; Pohlmeier *et al.* 1997; Ramon *et al.* 2004; Sadleir and Argibay 2007).

For decades a resistivity ratio 1:80:1 between the brain, skull and scalp has been considered as a standard value in EEG forward and inverse studies. This resistivity ratio was the outcome of research by Rush and Driscoll (1968, 1969). They assumed that the dry skull is an insulator and takes on a resistivity value which is directly proportional to that of the fluid with which it is permeated. In the measurements they found ratio values between 50 and 300 for the transverse skull resistivity and from 5 to 40 for parallel skull resistivity. The value 80 for the resistivity ratio between the skull and the fluid in the analytical three-layer spherical model gave the best correspondence to the measurement results made with the tank model including a human post mortem half-skull.

Already in the 1990s the large variation in skull resistivity was noted (Law 1993) and studies were conducted with different resistivity ratios than the 1:80:1 which was considered standard at that time. The purpose of these studies was not to discover a correct value for the skull resistivity but rather to emphasize the effect of misspecification of skull resistivity, e.g., in dipole localization studies (Pohlmeier *et al.* 1997).

Since 2000 there has been much research into defining the skull resistivity to be applied in the models and many papers have been published on the topic. A wide range of different methods have been applied to measure or estimate the skull resistivity. Some of these methods are based on measuring actual skull samples, some of which are post mortem (Akhtari *et al.* 2000; Oostendorp *et al.* 2000) and others live samples removed during surgery (Akhtari *et al.* 2002; Hoekema *et al.* 2003). A wide range of methods based on modelling the head as a volume conductor have also been applied to estimate the skull resistivity. Most of the modelling-based methods apply electrical impedance tomography (EIT) (Oostendorp *et al.* 2000; Goncalves *et al.* 2003a; Goncalves *et al.* 2003b; Hoekema *et al.* 2003). In addition, modelling-based methods exploiting subdural potential measurements have been studied (Lai *et al.* 2005; Zhang *et al.* 2006b). Combined resistivity estimation and source localization based on both electric and magnetic measurements have also been introduced (Goncalves *et al.* 2003a; Gutierrez *et al.* 2004).

From the different modelling-based studies it is evident that the proper effective resistivity values applied for different tissues depend firstly, on the types of tissues included in the model and, secondly, on the geometry of the model. The thicknesses of different tissue layers also influence the effective resistivity ratio (Lai *et al.* 2005; Nunez and Srinivasan 2006). Brain tissue has a higher resistivity than scalp tissue, and these realistic values are typically applied in the four-layer models, where the fourth layer presents the CSF (Ferree *et al.* 2000; Gutierrez *et al.* 2004). It is common that in three-layer models including the scalp, skull and brain, equal conductivity is assigned to the brain and scalp (Rush and Driscoll 1968; Oostendorp *et al.* 2000). This is justified by the fact that in the three-layer models, where the well conducting CSF is included in the brain

tissue, the effective resistivity of the combined brain and CSF is lower than the resistivity of brain tissue alone.

Tangential shunting of the current through the highly conductive CSF may cause additional spread of the scalp potentials, and thus in three-layer models a higher than realistic skull resistivity should be applied to compensate for the lack of CSF. Nunez and Srinivasan (2006) have shown in a forward EEG study that the three-layer spherical model and four-layer spherical head model with skull to brain resistivity ratios of 30:1 and 40 – 60:1, respectively, result in similar volume conductor effects. As stated, it is important that the effective resistivity ratios estimated in certain studies should be used for only models with similar geometries (Lai *et al.* 2005).

The realistic versus spherical geometry of the model may also affect the effective resistivity ratio. For example, Goncalves *et al.* (2003a, 2003b) estimated the resistivities with an EIT-based method both by applying a spherical and a realistically shaped three-layer head models. When the realistic BEM model was applied (Goncalves *et al.* 2003b), the average resistivity ratio between skull and brain was 42 with a relative standard deviation of 27 %. When the head was modelled with a layered spherical model (Goncalves *et al.* 2003a), the corresponding resistivity ratio was on average 72 with a relative standard deviation of 48 %. Goncalves *et al.* (2003b) report that if the systematic errors in the head models are large, the estimated resistivity values will tend to compensate for them. Thus more reliable estimates can be obtained by applying a patient-specific realistically shaped head model. In their studies the value for the skull to brain resistivity ratio was lower in a more realistically shaped head model than in a spherical model, though the reliability of the result was also lower in spherical geometry.

In many studies the dependence of the skull resistivity has been found to depend on the patient's age (Law 1993; Hoekema *et al.* 2003). Generally, the younger the patient, the lower the resistivity of the skull. Additionally, because of its structure, the resistivity varies between different locations of the skull (Law 1993). There is also clear evidence that the resistivity of a live skull is lower than that of a cadaver skull sample. Akhtari *et al.* (2002) observed that the resistivity ratio between post-mortem and live skull samples is 2.86. Studies conducted on femoral bone support the increase of resistivity in post mortem versus live skull samples. Kosterich *et al.* (1983) showed a resistivity ratio of 2 – 3 between post-mortem and fresh samples.

The reported resistivities of post mortem skull samples have varied between 13.6 Ωm and 435 Ωm (Law 1993; Akhtari *et al.* 2000; Oostendorp *et al.* 2000). The reported resistivities of live skull samples removed during surgery have varied between 12.5 Ωm and 117.6 Ωm, with a clear trend that the younger the subject, the smaller the resistivity value (Akhtari *et al.* 2002; Hoekema *et al.* 2003). In the modelling-based approaches the reported skull resistivity values have varied between 67 and 308 Ωm (Oostendorp *et al.* 2000; Goncalves *et al.* 2003a; Goncalves *et al.* 2003b). A summary of reported skull resistivity values is given in Table 3.1.

Instead of reporting only skull resistivity values, a wide range of studies have suggested new resistivity ratios for use in head volume conductor models. The summary of these is

given in Table 3.2. In addition to the ratios listed in Table 3.2, other revised values have also been applied during the last decade. For example, when modelling the four tissues of scalp, skull, CSF and brain, one commonly applied resistivity ratio is 14:1 for skull and brain and 24:1 for skull and scalp (Ferree *et al.* 2000; Grieve *et al.* 2004). In three layer models ratios of 1:16:1 (Im *et al.* 2007), 1:15:1 (Zhang *et al.* 2003; Yao and Dewald 2005), 1:20:1 (Zhang *et al.* 2006a) have been applied.

Table 3.1. Reported skull resistivity values.

| Method | Reference | Range of resistivity values [Ωm] | Average resistivity [Ωm] |
|---|---|---|---|
| post mortem skull | (Rush and Driscoll 1969) | | 178 |
| post mortem skull | (Oostendorp *et al.* 2000) | | 67 |
| post mortem skull | (Akhtari *et al.* 2000) | 171 - 435 | 300 |
| post mortem skull | (Law 1993) | 13.6 - 214 | 75.6 |
| post mortem skull | (Hoekema *et al.* 2003) | | 46.7 |
| live skull | (Akhtari *et al.* 2002) | 87.7 – 118 | 105 |
| live skull | (Hoekema *et al.* 2003) | 13 – 31 | 18 |
| model, 3-layer BEM | (Oostendorp *et al.* 2000) | | 76 |
| model, 3-layer BEM | (Goncalves *et al.* 2003b) | 81.2 – 142 | 122 |
| model,3-layer spherical | (Goncalves *et al.* 2003a) | 133 - 308 | 204 |

Table 3.2. Estimated resistivity ratios.

| Model | Reference | RESISTIVITY RATIO | | | | |
|---|---|---|---|---|---|---|
| | | scalp | | skull | | brain |
| | (Akhtari *et al.* 2002) | 1 | : | 18 | : | 1 |
| | (Hoekema *et al.* 2003) | 1 | : | 8 | : | 1 |
| 3-layer spherical | (Rush and Driscoll 1969) | 1 | : | 80 | : | 1 |
| 3-layer spherical | (Goncalves *et al.* 2003a) | 1 | : | 72 | : | 1 |
| 3-layer spherical | (Lai *et al.* 2005) | 1 | : | 25 | : | 1 |
| 3-layer BEM | (Oostendorp *et al.* 2000) | 1 | : | 15 | : | 1 |
| 3-layer BEM | (Goncalves *et al.* 2003b) | 1 | : | 20-50 | : | 1 |
| 3-layer FEM | (Zhang *et al.* 2006b) | 1 | : | 19 | : | 1 |

## 3.4 Improvement of the spatial resolution of EEG

### *3.4.1 Spatial resolution of EEG*

Various studies have been conducted on methods to improve the spatial resolution of EEG recorded from the surface of the scalp. Some studies consider only the application of spatial enhancement methods, while a second group of studies deal exclusively with the effect of increasing the number of measurement electrodes. A third group of studies have been devoted to studying the combined effect of these two factors. There are only a few studies in which numerical values for spatial resolution have been defined.

The term spatial resolution has been applied in the literature somewhat inconsistently. In some studies the term refers to localization accuracy and in other studies to

distinguishing between two sources. Bradshaw *et al.* (2001) described these two approaches as localization resolution and imaging resolution and concluded that these are two different measures of spatial resolution. Wang and He (1998) studied the spatial resolution of a cortical imaging method and defined the spatial resolution as the minimal distance between two radial dipoles when the reconstructed cortical potentials can separate the two areas of activity. The criterion for the separation was determined by detecting whether there is a valley between the two areas of activity. Bradshaw *et al.* (2001) suggested that the Rayleigh criterion could be used to define the spatial resolution. According to this criterion, two sources can be resolved if the minimum of the valley between the two peaks is less than 0.81 times the maximum of the two peaks. Malmivuo and Suihko (2004) and Ferree *et al.* (2001a) used half-sensitivity volume (HSV) to determine the spatial resolution. The concept of HSV was introduced by Malmivuo *et al.* (1997). The HSV is defined as the volume within the brain in which the magnitude of the sensitivity is greater than half of its maximum value within the brain.

### *3.4.2 Distributed source models and cortical imaging*

The first spatial enhancement methods were based on the application of the surface Laplacian operator. This is also the simplest and most widely applied spatial enhancement method (Gevins *et al.* 1995). Most of the Laplacian methods assume, for example, that skull thickness and resistivity are constant everywhere in the head. On this assumption, the surface Laplacian can be estimated as proportional to the cortical potential distribution. As Nunez *et al.* (1994) demonstrate, this holds for three-layer spherical head models. However, in a four-layer model, the surface Laplacian becomes a less accurate measure of cortical potentials as the CSF thickness increases. This is caused by additional spreading of source current by the CSF.

In the surface Laplacian methods, the second spatial derivative of the scalp potential distribution is calculated on a two-dimensional scalp surface. The operator estimates the orthogonal current flow through the skull at each scalp location. The surface Laplacian methods act as a bandpass filter (Nunez *et al.* 1994; Nunez and Srinivasan 2006) and thus they are generally believed to solve the generators of the cortical origin and to be insensitive to subcortical generators (Perrin *et al.* 1987; Law *et al.* 1993a; Law *et al.* 1993b; Nunez and Srinivasan 2006).

The surface Laplacian was first applied to scalp EEG by Hjort (1975). His method is a so-called local Laplacian method, because the surface Laplacian at each electrode location is calculated on the basis of the potential value at that electrode location and its neighbouring electrode locations. Thus the local Laplacian cannot be solved in the peripheral electrodes. In the local methods, the scalp surface is approximated as a planar surface. So-called global or spline Laplacian methods have subsequently been developed (Babiloni *et al.* 2001b). The global methods are based on the application of spline interpolation functions to the scalp potentials and then evaluating the surface Laplacian of the spline function. Thus the solution is not limited to electrode locations. In global methods the Laplacian at each location is estimated on the basis of the potentials at all electrode locations. Spline methods were originally developed for spherical and ellipsoidal surfaces (Perrin *et al.* 1987; Law *et al.* 1993a).

In the 1990s so-called realistic surface Laplacian methods taking into account the realistic scalp shape were developed. The scalp surface has been estimated either from the measured electrode locations (Le *et al.* 1994) or from the patients' MR images (Babiloni *et al.* 1996; Babiloni *et al.* 1997a; Babiloni *et al.* 1998) or CT images (He *et al.* 2001). A method has also been developed in which the effect of variation in the scalp thickness has been considered (Babiloni *et al.* 1997a). Babiloni *et al.* (1996) showed that Laplacians calculated on realistic scalp surfaces are more precise that those calculated on spherical or ellipsoidal surfaces. Laplacian methods have been mainly validated by evoked potential measurement, the most common of them being somatosensory evoked potentials (Perrin *et al.* 1987; Law *et al.* 1993b; Le *et al.* 1994; Babiloni *et al.* 1996; Babiloni *et al.* 1997a; Babiloni *et al.* 1998; He *et al.* 2001).

During the last two decades spatial enhancement methods, which are based on the application of the volume conductor model of the head, have been developed. These methods include, for example, the so-called cortical imaging technique and the spatial deblurring method.

The cortical imaging technique is a mathematical imaging method for simulating cortical surface potentials. It was introduced by Kearfott *et al.* (1991) and further studied by Sidman *et al.* (1992). In the original CIT the head was modelled with a homogeneous spherical volume conductor model. The sources were presented as a hemispherical layer of radially oriented current dipoles, which was located inside the cortical surface. The strengths of the dipole sources were solved inversely from scalp EEG and from the estimated strengths the cortical potential distribution was solved as a forward solution. Wang and He (1998) made improvements to CIT and studied the method with extensive simulations. First they replaced the homogeneous volume conductor model with a three-layer inhomogeneous model. They replaced the hemispherical dipole layer with a spherical dipole layer. They also defined numerical values for spatial resolution. They concluded that in a three-layer spherical head model, where the relative skull resistivity is 80, the spatial resolution obtained with 128 electrodes is 1.2 cm and 1.4 cm in the presence of 5 % and 10 % noise, respectively. The CIT has been further extended by Babiloni *et al.* (1997b) who applied a realistic inhomogeneous boundary element head model and also by Zhang *et al.* (2006a) who applied a finite element head model.

The drawback of most CIT-based methods is that they are indirect. First, the strength of the equivalent dipole layer is inversely estimated from the scalp data. Only after that, however, is the cortical potential distribution solved as a forward solution on the basis of the estimated equivalent dipole layer strength. To overcome this, He *et al.* (2002a) presented a cortical equivalent dipole layer imaging method. They demonstrated that both cortical and subcortical brain activity can be equivalently represented by a closed cortical dipole layer. They showed that the cortical imaging can be performed by inversely calculating the strength of the equivalent dipole layer.

There also exist cortical imaging methods which directly relate the cortical and scalp potentials. Edlinger *et al.* (1998) have derived an analytical solution to cortical potentials in a multishell volume conductor model. Some of these methods are based on the Barr's boundary element method developed for epicardial imaging (Barr *et al.* 1977). Srebro *et*

*al.* (1993) applied the Barr's method to a homogeneous spherical head model. He *et al.* (1999) modified the Barr's method by first deriving the equations for an inhomogeneous head model. They also developed a numerical adaptive algorithm which improves the accuracy of the method. The adaptive algorithm takes particular account of the effect of thin low-conductive skull layer. Their method has been applied both to spherical head models (He *et al.* 1999; Zhang *et al.* 2003) and realistic head models (He *et al.* 2002b).

Another widely studied method that directly relates the cortical and scalp potentials is called deblurring, and this was developed by the research group of Gevins (Gevins *et al.* 1999). The cortical potential distribution is calculated on the basis of the scalp potential distribution using a realistically shaped finite element model of the patient's head. The model includes scalp, skull and cortical surfaces. The cortical potentials are estimated with a multidimensional optimization method. Ollikainen *et al.* (2001) have also applied a finite element method to cortical imaging, though their solution is based on a Bayesian method. The deblurring method has been applied both for evoked response studies and for higher cognitive brain function studies (Gevins *et al.* 1991; Le and Gevins 1993; Gevins *et al.* 1994; Gevins *et al.* 1996; Gevins *et al.* 1999).

The different spatial enhancement methods have been verified either with simulated or experimental data. Many different evoked potential studies have been conducted to evaluate and validate the improvement in spatial resolution obtained with spatial enhancement methods. In the case of evoked potential studies, some knowledge of the underlying neural generators exists, and the locations of these have been compared to the solved cortical source distribution (Gevins *et al.* 1991). Of great importance in the development and evaluation of cortical imaging methods are the actual cortical potential measurements. In earlier studies evoked potential measurements were conducted, but the cortical potentials and scalp potentials were not recorded simultaneously. SEPs generated by median nerve stimulation were applied by Sidman *et al.* (1992) when evaluating the CIT and also by He *et al.* (2002b), when evaluating their cortical potential imaging method. SEPs elicited by steady-state finger stimulation have been applied in the evaluation of the deblurring method (Le and Gevins 1993; Gevins *et al.* 1994).

Epileptic patients have been widely studied when validating different spatial enhancement methods. In earlier studies, the locations of epileptic foci were verified, for example, by surgery and these locations were compared to the solved cortical potential distribution (Sidman *et al.* 1992; Zhang *et al.* 2003). Zhang *et al.* (2006a) were the first to apply simultaneously measured data from the cortex and scalp. They measured interictal epileptiform spikes from a pediatric patient, when evaluating the performance of CIT. The subdural low conducting electrode grid was also included in their volume conductor model. Gevins *et al.* (1999) have discussed the application of deblurring and cortical imaging in general in studying epileptiform phenomena. They propose that deblurring can better characterize the distribution of epileptiform phenomena. They also report that the method can help in optimizing the locations for subdural grids and also that it might be almost as good as grid localization methods, at least for surgical planning purposes.

The advantages of the cortical imaging methods have been widely studied in conjunction with the advantages of increasing the number of measurement electrodes. Many studies

have also included the effect of measurement noise in evaluation of the improvements. These results are discussed further in the next section.

### *3.4.3 Number of EEG electrodes in improving spatial resolution*

Since the beginning of the 1990s several studies have investigated the benefits of increasing the number of EEG electrodes. The first possible approach is to study the forward solution of EEG and to evaluate the number of electrodes needed to accurately sample the potentials on the surface of the scalp (Gevins *et al.* 1990; Srinivasan *et al.* 1996; Srinivasan *et al.* 1998; Grieve *et al.* 2004). The second apparent approach is to study how the number of electrodes affects the accuracy of inverse solutions. In the case of inverse solutions, the effect of the number of electrodes on both improving the source imaging accuracy (Wang and He 1998; He *et al.* 1999) and source localization accuracy (Liu *et al.* 2002; Lantz *et al.* 2003; Michel *et al.* 2004) has been studied. In these studies both spherical head models and realistically shaped head models have been applied. It should be noted that in most of the studies the applied value for skull resistivity has been 80 times that of scalp and brain. In several articles, an increase in the number of electrodes to at least 128 has been shown to improve the accuracy of the results (Gevins et al. 1990; Srinivasan *et al.* 1996; Babiloni *et al.* 1997b; Srinivasan *et al.* 1998; Wang and He 1998).

*RESULTS BASED ON FORWARD EEG SOLUTION*

One approach to study the need for dense sampling of potentials on the scalp surface is to estimate the effect of blurring caused by volume conduction. Gevins *et al.* (1990) achieved this by calculating the point spread function of radial cortical activity on the surface of the scalp by applying a four-layer spherical head model. They calculated that the 3dB point of the point spread function was 2.5 cm, which gives the interelectrode distance needed to accurately sample the scalp potentials. Presumably, because the study was conducted already in 1990, the resistivity of the skull was 80 times that of brain and scalp. Depending on the electrode system, the interelectrode distance of 2.5 cm corresponds to approximately 128 electrodes.

Srinivasan *et al.* (1996) estimated the required spatial sampling of scalp EEG data by studying the spatial power spectrums. They applied a four-layer spherical head model in their study. They concluded, on the basis of both simulations and experimental data, that in potential field mapping of the scalp the required electrode density is an interelectrode distance of 2.7 cm. For the surface Laplacian they concluded that improved accuracy can be achieved when the interelectrode distance is reduced to 2.0 cm. In this study they investigated the spatial power spectra as a function of spherical harmonic degree.

In (Srinivasan *et al.* 1998) similar methods were applied as in (Srinivasan *et al.* 1996) and also the sampled scalp surface potential distributions were visualized. They examined the Geodesic electrode system of 128 electrodes and also down-sampled montages of 64, 32 and 19 electrodes. Using a simulation study they concluded that at least 128 electrodes are needed to correctly sample the scalp potentials generated by cortical current sources. Their study conducted with the experimental data gave similar results.

Grieve *et al.* (2004) studied the spatial sampling error of scalp potentials with Geodesic electrode nets including 64, 128 and 256 electrodes. In their study they applied a four-layer spherical head model for both adult and infant heads. They applied a more realistic value for skull resistivity, which was 24 times the resistivity of the scalp and 14 times that of the brain. The general trend of their results showed that an increase in the number of electrodes reduces the error. They conducted their study both in the absence of measurement noise and with power SNR of 10. The 256 electrode system achieved highest accuracy in the absence of measurement noise. In the presence of noise, the 128 and 256 electrode systems resulted in similar error which was only slightly smaller than the error obtained with 64 electrodes. They concluded that the error obtained with 64 electrodes in the noiseless case was below 10 %, though they cautioned that this error level might be unacceptable, for example, in source localization studies.

*RESULTS BASED ON INVERSE EEG SOLUTION*

Lantz *et al.* (2003) studied the number of electrodes that are needed to localize interictal epileptic sources. They measured the clinical EEG with 123 electrodes and also examined the subsets of 31 and 63 electrodes. They also studied the number of electrodes from simulations in which the number was varied between 25 and 181. From their clinical data they conclude that localization accuracy is substantially better with 63 than with 31 electrodes and that there is still improvement when the number of electrodes is increased from 63 to 123. The results of the simulation study supported this result.

Michel *et al.* (2004) published an extensive review on source imaging methods and discussed, for example, the various factors influencing the accuracy of source imaging. One of the factors discussed the number of electrodes. In their paper they conclude that if single focal sources are assumed, the increase in the number of electrodes up to approximately 60, as in Lantz *et al.* (2003), will suffice for accurate source localization. On the basis of the results of a simulation study, the authors also conclude that fully distributed inverse solutions benefit from a larger number of electrodes. They approximated the number of electrodes needed as at least 100.

Liu *et al.* (2002) conducted a simulation study of the localization accuracy of a source imaging method with EEG, MEG and combined EEG/MEG. In the case of EEG, they compared the accuracy of 30 and 61 electrode systems in the presence of noise. They applied a realistically shaped head model with a resistivity ratio of 1:80:1 for brain, skull and scalp. The root mean square SNR was 10 and it was observed that the increase in the number of electrodes improved the localization accuracy of EEG.

Babiloni *et al.* (2001a, 2004) also investigated the multimodal integration of EEG and MEG data in improving the accuracy of inverse cortical current source estimates. They evaluated the accuracy of the methods within predefined regions of interest (ROI). Both papers also compared certain EEG electrode systems. However, neither paper makes any reference to the resistivity ratio between the tissues. In both studies a boundary element model of the head was applied. In a simulation study they evaluated how well the cortical activities could be reconstructed on predefined regions of interest on the cortical surface. Babiloni *et al.* (2001a) employ three different indexes of the resolution matrix as

a criterion. Their study evaluates the difference between 121-channel and 61-channel EEG. In terms of all three applied indexes, the 121 channel EEG performed better than the 61 channel EEG in solving the weighted minimum norm source estimates of measured evoked potentials. In another paper (Babiloni *et al.* 2004) the main interest was on the effect of signal-to-noise ratio and also the effect of sensor number on the accuracy of the inverse solution. In this study the relative error and correlation coefficient were applied to assess the accuracy of different solutions. EEG systems including 128, 61 and 29 electrodes were studied. From the results of a simulation study it could be observed that with power SNRs varying between 1 and $\infty$, the accuracy of the 128 electrode system was only slightly better than the accuracy of the 61 electrode system. The accuracy of the 128 electrode system was more affected by noise than that of the 61 electrode system.

The effect of increasing the number of electrodes to improve the accuracy of surface Laplacian has been investigated by several authors. In most cases, the effect of increasing the number up to 128 has been reported (Law *et al.* 1993a; Nunez *et al.* 1994; He *et al.* 2001). The general trend in the results is that an increase in the number of electrodes increases the accuracy of the results, even in the presence of measurement noise (He *et al.* 2001). Furthermore, the effect of increasing the number of electrodes up to 256 has been found to increase the accuracy of surface Laplacians in the presence of noise in simulation experiments (Babiloni *et al.* 1995, 1996). Babiloni *et al.* (1996) examined how an increase in spatial sampling improved the accuracy of the realistic surface Laplacian estimate. They discovered that increasing the number of electrodes up to 128 resulted in an increase in the spatial information content of the surface Laplacians of movement related evoked potentials. In a simulation study they compared the realistic Laplacian to analytical Laplacian in a spherical model and found that an increase in the number of electrodes up to 256 resulted in improved accuracy of the realistic Laplacian estimate in the presence of measurement noise. However, it has been reported that in certain cases the increase in the number of electrodes distorts the solution of spline Laplacians. Le *et al.* (1994) have reported that the application of a dense electrode montage and a spline Laplacian method may lead to inaccurate results. Babiloni *et al.* (1995) have observed that the higher the number of electrodes, the more the Laplacian calculated using spherical scalp model deviates from the Laplacian calculated using a realistically shaped scalp model.

Nunez *et al.* (1994) studied the accuracy of two different methods, the surface Laplacian and cortical imaging, in improving the spatial resolution of EEG. In their simulation study conducted with three- and four-layer spherical head models, the accuracy of the methods was improved as the number of electrodes is increased from 48 to 64 and from 64 to 118.

Wang and He (1998) studied, for example, the effect of increasing the number of electrodes on the accuracy of CIT. They applied a three-layer spherical head model with a resistivity ratio of 1:80:1 and investigated electrode systems consisting of 16, 40, 128 and 301 electrodes. From their results they conclude that in CIT the application of 128 electrodes seems reasonable for improving the accuracy of cortical potential distribution from a practical point of view. However, a slight improvement on the accuracy for superficial sources was observed when the number of electrodes increased to 301. In their study the noise level was either 5 % or 10 %.

He *et al.* (1999) studied a cortical potential imaging method based on a boundary element method. They applied a resistivity ratio of 1:80:1. In their simulation they considered 65, 128, 310 and 640 electrodes placed on the upper hemisphere of the model and in every simulation 310 electrodes performed better than 128 electrodes. The noise level in their study was 10 %. It should also be mentioned that source eccentricity was 0.65. The radii of the model were 1.0, 0.92 and 0.87. Such deep sources produced quite widely spread potential distributions on the cortical surface and thus may not require the highest possible sampling of the potentials.

Gevins *et al.* (1994) studied the effect of the number of electrodes on the accuracy of the deblurring method. They conducted measurements with 124 electrodes on the scalp surface. They performed a simulation study by applying an individual realistic finite element head model and concluded that a denser electrode array on the scalp surface could further increase the spatial resolution of the cortical potentials estimated with their method. Babiloni *et al.* (1997b) also studied the effect of increasing the electrodes with a model-dependent spatial deblurring method. Their results showed that increasing the number of electrodes from 28 to 64 and to 128 increased the accuracy of calculated dura potentials.

## 3.5 Sensitivity distribution of EEG measurement leads

### *3.5.1 Lead field and reciprocity theorem*

An important aspect in EEG as well as in other measurements of bioelectric activity is to understand where within the volume conductor the signal measured with a certain lead is most likely generated. This can, for example, be achieved by studying the measurement sensitivity distribution of an EEG lead. Lead field theory together with the reciprocity theorem provides a convenient method to study the sensitivity distributions. The lead field in the volume conductor can be calculated by feeding a unit current to the lead, according to the reciprocity theorem of Helmholtz. The reciprocal current gives rise to a current density field which is equivalent to the distribution of the sensitivity of the lead (Malmivuo and Plonsey 1995).

Equation (3.10) describes the relationship between the measured signal $V_L$ in the lead and the current sources $\mathbf{J}^i$ in the volume conductor, when a unit reciprocal current $I_r$ is applied to the lead (Malmivuo and Plonsey 1995).

$$V_L = \frac{1}{I_r}\int \frac{1}{\sigma}\mathbf{J}_L \cdot \mathbf{J}^i dv\,, \tag{3.10}$$

where $\mathbf{J}_L$ is lead field current density, $\mathbf{J}^i$ is the current source density and $\sigma$ is the conductivity of the volume conductor at the source location. The reciprocity and lead field theorems are illustrated in Figure 3.5.

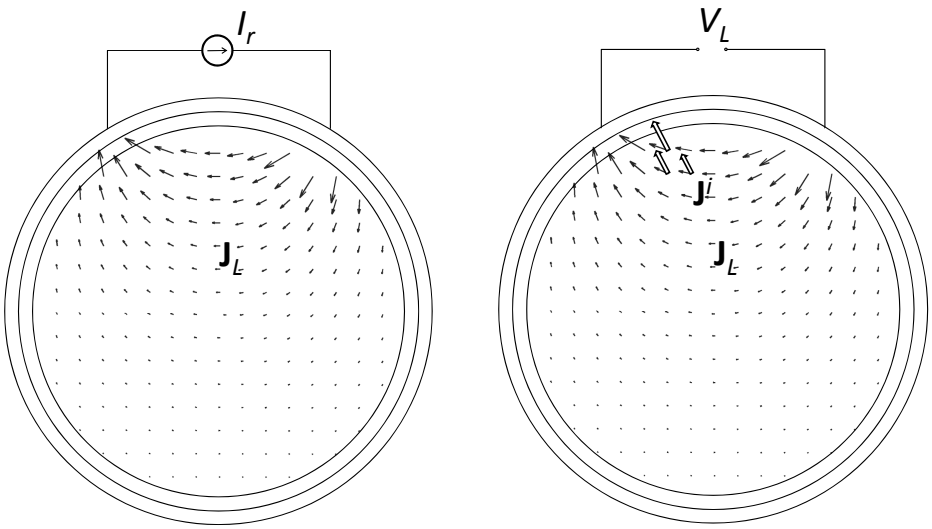


Figure 3.5. Reciprocity and lead field theorems. a) The reciprocal current $I_r$ gives rise to a current density field $\mathbf{J}_L$, which is the lead field. b) The voltage $V_L$ measured with the lead is obtained by integrating the dot product of the lead field, divided by the conductivity and impressed current density $\mathbf{J}^i$ (illustrated by white arrows) over the volume source according to Equation (3.10).

In Figure 3.5 the lead field is illustrated as a field of lead vectors. The lead field theory introduced by McFee and Johnston (1953, 1954a, 1954b) is an extension of the lead vector theory introduced by Burger and Van Milaan (1946, 1947, 1948).

The lead vector is defined as a three-dimensional transfer coefficient which gives the relationship between the source dipole and the measured voltage in the lead. The value of the lead vector depends on the location of the measurement lead, the shape of the volume conductor, the distribution of the resistivity within the volume conductor and on the location of the source. Through superposition the measured lead voltage generated by a single source at a fixed location can be calculated as a dot product between the lead vector $\mathbf{c}_L$ and the source dipole $\mathbf{p}$

$$V_L = \mathbf{c}_L \cdot \mathbf{p} \tag{3.11}$$

If the lead vectors are calculated for each point within the volume conductor, they form a continuous vector field, which is the lead field. In this case the measured lead voltage is calculated with Equation (3.10).

Rush and Driscoll (1968, 1969) derived a set of equations for calculating the reciprocally energized potential distribution $\phi$ within a three-layer spherical head. The lead field can be calculated from the potential distribution with

$$\mathbf{J}_L = -\sigma \nabla \phi \tag{3.12}$$

### *3.5.2 Sensitivity distribution of two-electrode EEG*

The sensitivity distributions of EEG leads were first studied by Rush and Driscoll (1968, 1969) and later by Malmivuo *et al*. (1997), Malmivuo and Suihko (2004) and also by Ferree *et al*. (2001a). In all these studies two-electrode EEG leads were investigated by varying the distance between the electrodes. The sensitivity distribution of each lead within the head model was studied with the reciprocal approach. The magnitude and orientation of the sensitivity distribution depends on the electrode distance and on the properties of the volume conductor. The results of these studies show that the sensitivity of a two-electrode lead is concentrated just below the measurement electrodes. The two-electrode lead is the most widely applied EEG lead.

The sensitivity distribution can also be applied to study the spatial resolution of scalp EEG. For this purpose Malmivuo *et al.* (1997) introduced the concept of HSV as described in section 3.4.1. The HSV describes how concentrated the sensitivity distribution of the lead is. The more concentrated the measurement sensitivity is, the better is the spatial resolution. Malmivuo and Suihko (2004) and Ferree *et al.* (2001a) studied the spatial resolution of EEG in a noiseless situation by applying a three-layer spherical head model and a four-layer spherical head model, respectively. They both studied the effect of electrode distance and skull resistivity on the spatial resolution. Malmivuo and Suihko (2004) found that with the new realistic skull resistivity values, the spatial resolution of EEG was much superior to that obtained if the relative skull resistivity is 80. Their results also indicate that if the relative skull resistivity is low there is still an improvement in spatial resolution when the interelectrode distance is as small as 10 mm.

Ferree *et al.* (2001a) introduced also the concept of the depth of the sensitivity distribution, which they defined as the maximum depth of all the points within the HSV. When the skull to scalp resistivity ratio was 24:1 and 80:1, the maximum depth was 2.6 cm and 3.7 cm, respectively. This concept further clarifies that the scalp-EEG recorded with a two-electrode leads detects mainly cortical activity.

### *3.5.3 Modifications of sensitivity distributions*

When the EEG sources are not located on the cortex the sensitivity distribution of a two-electrode lead is not optimal for measurement purposes. The synthesisation of improved sensitivity distributions has already been described by McFee and Johnston (1954b), who modified the lead fields for detecting the equivalent heart vector in the case of ECG. They showed how the lead fields can be modified with such a lead where both of its terminals are connected with any number of resistors to electrodes on the surface of the body. The synthesized leads consisted, as an example, of four electrodes. Brody (1957) later introduced a method to synthesize a uniform sensitivity distribution within a homogeneous finite volume conductor. When the sensitivity distribution is uniform, it has unvarying magnitude and direction through the volume conductor. A uniform sensitivity distribution is ideal for the detection of each orthogonal component of the electric dipole moment of a volume source.

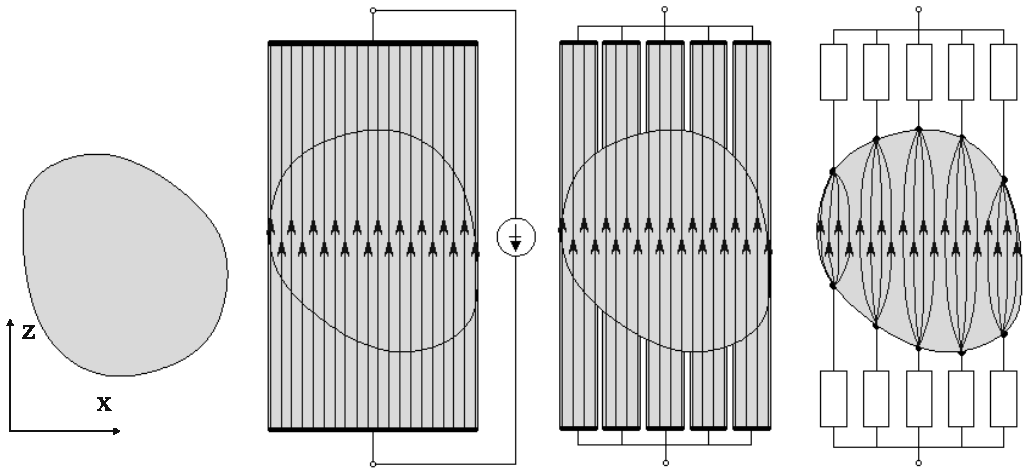


(a) (b) (c) (d)

Figure 3.6. A method to synthesize a uniform lead field in a finite homogeneous volume conductor in the direction of the z-axis. Modified from Malmivuo and Plonsey (1995).

The method for synthesizing a uniform lead field in a finite homogeneous volume conductor has been described in detail by Malmivuo and Plonsey (1995). The generation of such a lead field is illustrated in Figure 3.6, where the uniform lead field is generated in the direction of a z-axis. In (a) an arbitrarily shaped infinite homogeneous volume conductor is presented. The volume conductor is extended in the direction of the z-axis, so that it forms a cylinder. The cross section of the cylinder in the xy-plane is the same as in the original volume conductor. If the two endings of the cylinder in the xy-plane are covered with electrodes, and a reciprocal current is applied to the lead, the lead field in the volume conductor is uniform, as illustrated in Figure 3.6 (b). In Figure 3.6 (c), the extensions of the volume conductor are sliced to form isolated filaments. The slicing does not alter the form of the lead field because it is done along the current flow lines so that they are not intersected. In Figure 3.6 (d), the volume conduction filaments outside the volume conductor are replaced with resistors. These resistors have the same resistive value as the corresponding isolated filaments. If a reciprocal current is applied through this resistor network, the lead field in the original volume conductor will be close to uniform. The greater the number of electrodes that are placed at the surface of the volume conductor, the more uniform is the sensitivity distribution.

In a homogeneous cylindrical volume conductor which has a circular cross section, e.g., in a thin disk, the uniform lead field is obtained when the reciprocal current injected at every electrode is incrementally proportional to $\cos\theta$, as illustrated in Figure 3.7 (Malmivuo and Plonsey 1995).

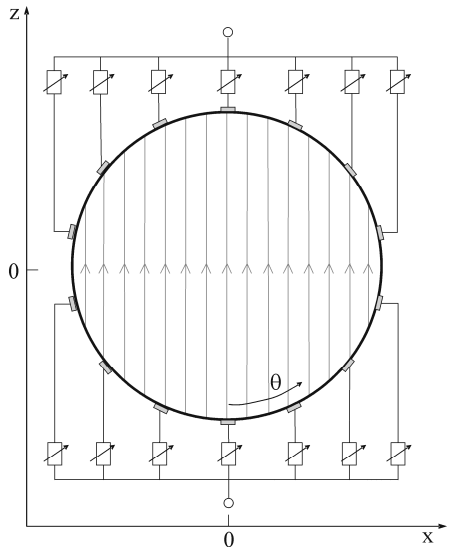


Figure 3.7. Synthesization of a uniform lead field within a thin disk. The electrodes are uniformly distributed on the surface of the disk. When the reciprocal current at every electrode is proportion to $\cos\theta$, the uniform lead field will be oriented along the positive z-axis (Malmivuo and Plonsey 1995).

# 4 MATERIALS AND METHODS

The present thesis adopts two different approaches to the application of multichannel EEG. Except for the applied volume conductor model, the methods applied in the two approaches are different and thus they are considered individually in their own separate sections. Chapter 4.3 presents the methods in the analysis of the spatial resolution of the cortical potential distribution and Chapter 4.4 presents the methods to improve the signal quality of deep EEG sources.

## 4.1 Volume conductor model

A three-layer spherical head model was applied in all of the publications. The geometry was adopted from Rush and Driscoll (1969). The model included the layers of scalp, skull and brain. The radii of the spheres were 92 mm, 85 mm and 80 mm, respectively. All of the tissues were assumed to be purely resistive and isotropic. One of the research topics was to study the effect of skull resistivity on the spatial resolution of EEG. Thus different values for the skull resistivity were applied, while the resistivities of scalp and brain were kept constant. The resistivity of the scalp was either 230 Ωcm (Geddes and Baker 1967; Laarne 2000) [I-III] or 222 Ωcm (Rush and Driscoll 1969) [IV-VII]. The resistivity of the brain was 222 Ωcm (Rush and Driscoll 1969) [IV-VII]. The resistivity of the skull varied between 222 Ωcm and 18400 Ωcm so that the resistivity ratio between scalp, skull and brain varied from 1:1:1 to 1:80:1. The applied resistivity ratios are listed in Table 4.1.

Table 4.1 Resistivity ratios between scalp, skull and brain applied in the publications.

| Resistivity ratio | Reference | Publication |
|---|---|---|
| 1:1:1 | | V |
| 1:8:1 | (Hoekema *et al.* 2003) | III, V |
| 1:15:1 | (Oostendorp *et al.* 2000) | I-VII |
| 1:30:1 | (Lai *et al.* 2005) | III, V |
| 1:80:1 | (Rush and Driscoll 1968) | III, V |

## 4.2 EEG electrode systems

The objective in [I-III] was to study how the electrode density affects the spatial resolution obtained at the cortical surface. The electrode systems that were studied included the 10-20 system consisting of 21 electrodes and the systems of 64, 128, 256

and 512 electrodes. Based on Gevins *et al.* (1991, 1994) and approximation in the case of 512 electrodes, the interelectrode distances in these systems were 60 mm, 33 mm, 23 mm and 16 mm and 11 mm, respectively. According to the electrode distance, the electrodes were uniformly placed over the entire scalp surface. These extended electrode systems were applied because they made it possible to study how densely the electrodes should be placed on the scalp in order to solve the underlying cortical potentials as accurately as possible. The resulting numbers of electrodes in the extended electrode systems were 34, 104, 232, 462 and 938, corresponding to the above-mentioned existing systems.

In [VI] and [VII] multielectrode EEG leads were studied. The leads were divided into two groups. The first group were so-called theoretical multielectrode leads, because the electrodes were placed uniformly over the entire spherical scalp surface. The numbers of electrodes in this group of leads were 58, 102 and 202. The second group were so-called experimental multielectrode leads because the electrode locations were those in a 124-channel EEG-cap (Neuroscan Quik-Caps).

## 4.3 Spatial resolution of cortical potential distribution [I-III]

### *4.3.1 Setting up the system of equations*

To obtain the forward transfer matrix **A** between the cortical potentials **x** and measured EEG potentials **b** in Equation (3.2), an FDM model of the spherical head model was constructed in [I - III]. The resolution of the model was 1.0 mm *x* 1.0 mm *x* 1.0 mm and it consisted of 3 341 112 nodes in the FDM resistor network. To reduce the computational load of the forward solutions, the cortical surface was so defined as to form a closed surface. The volume inside this surface could thus be omitted and the volume conductor consisted of the volume between closed cortical and scalp surface, as illustrated in Figure 3.3. The reduced volume conductor model consisted of 1 204 456 nodes, of which 67 640 were located on the cortical surface. To further reduce the computational load of the forward transfer matrix, groups of adjacent nodes were combined to form approximately equally-sized source areas on the cortical surface. The number of source areas varied between 52 and 8450 in [I - II] and was 8450 in [III]. The potential at each node within one source area was kept constant.

The forward transfer matrices were solved with the FDM solver (Takano 2002). The sparser electrode systems were defined as a subset of the 512 electrode system and the larger source areas were formed by combining adjacent source areas. Thus it was necessary only to calculate the forward transfer matrix corresponding to the largest number of electrodes and source areas. The different skull resistivities modified the FDM model, and thus new forward solutions, were calculated for models with different skull resistivities; altogether four different full forward transfer matrices were solved corresponding to the relative skull resistivities of 8, 15, 30 and 80.

### 4.3.2 Finite difference method

The software used for the FDM calculations [I-III] was originally developed by Walker (Walker 1985; Walker and Kilpatrick 1987) at the University of Tasmania. At the Ragnar Granit Institute the software has been further developed by Hyttinen (1994) and Kauppinen *et al.* (1999). The present version has been developed by Takano (2002). The validity of FDM applied in the calculation of the electric fields in the brain has been studied by Laarne *et al*. (1995). It was shown that the accuracy depends on the grid size and the 2 mm *x* 2 mm *x* 2 mm grid provides high enough accuracy. FDM was applied instead of using analytical methods because in future studies the realistic model can be easily constructed from segmented MR images (Kauppinen *et al.* 1999; Laarne *et al.* 1999).

In the applied FDM, each pixel of a head image data represents a voxel. Two dimensions of the voxel are defined from the image data and the third dimension is obtained from the spacing between the image slices. Resistivity of a voxel is defined as the resistivity of the tissue in question. The finite difference mesh is formed by placing the nodes at the vertices of each voxel. The conducting volume between adjacent nodes is replaced by an equivalent resistor. The value of each resistor depends on the resistivities of four surrounding voxels and their dimensions. The difference equations between adjacent nodes are set up by applying Ohm's and Kirchoff's laws. The source nodes are defined by assigning them potential values. (Walker 1985; Kauppinen *et al.* 1999)

### 4.3.3 Analysis of the accuracy of cortical potential distribution

The estimation of the spatial resolution of cortical potential distribution was based solely on studying the forward transfer matrices. Thus no inverse problems constrained to certain EEG data were solved. All calculated forward transfer matrices corresponding to different skull resistivity values, different number of electrodes and different number of source areas, were decomposed with SVD. The normalized singular values $\sigma_i/\sigma_1$ were plotted for each matrix to define the truncation point according to Equation (3.9). The steepness of these curves describes how ill-conditioned the forward transfer matrices are. The more ill-conditioned the system is, the more regularization is needed when the inverse problem is solved. Those normalized singular values $\sigma_i/\sigma_1$, whose magnitude is smaller than the relative noise level must be truncated to zero. The basis vectors of the source space corresponding to the truncated singular values cannot be reconstructed. The procedure in the estimation of the spatial resolution of cortical potential distribution is illustrated in Figure 4.1.

In the study series the purpose was also to estimate the realistic noise levels which are present in EEG measurements. The estimation of the noise level was conducted on the basis of the idea that when the purpose is to inversely solve the cortical potential distribution, the actual signal consists of all activity generated within the brain, and the noise is composed of other bioelectric signals, electrode contact noise, instrumentation noise and noise coupled from the environment.

The estimation of the combined effect of the latter three of these components was conducted in [II]. For this purpose two different types of measurement were studied. The first set of measurements is called knee measurements because they were conducted by placing electrodes on the knee of a subject. It is erroneously written in [II] that Ag-AgCl electrodes were applied, though in reality they were tin electrodes. Because of the anatomy of the knee, the contribution of EMG to the measured signal can be assumed to be relatively small. The second set of measurements was provided by the Tampere University Hospital, and the data consisted of burst-suppression data measured under anaesthesia. The EEG measurements were conducted with a 10-20 –system using Ag-AgCl electrodes. During suppression**,** the signal is mainly composed of the noise components because the contribution of brain activity in the signal is low.

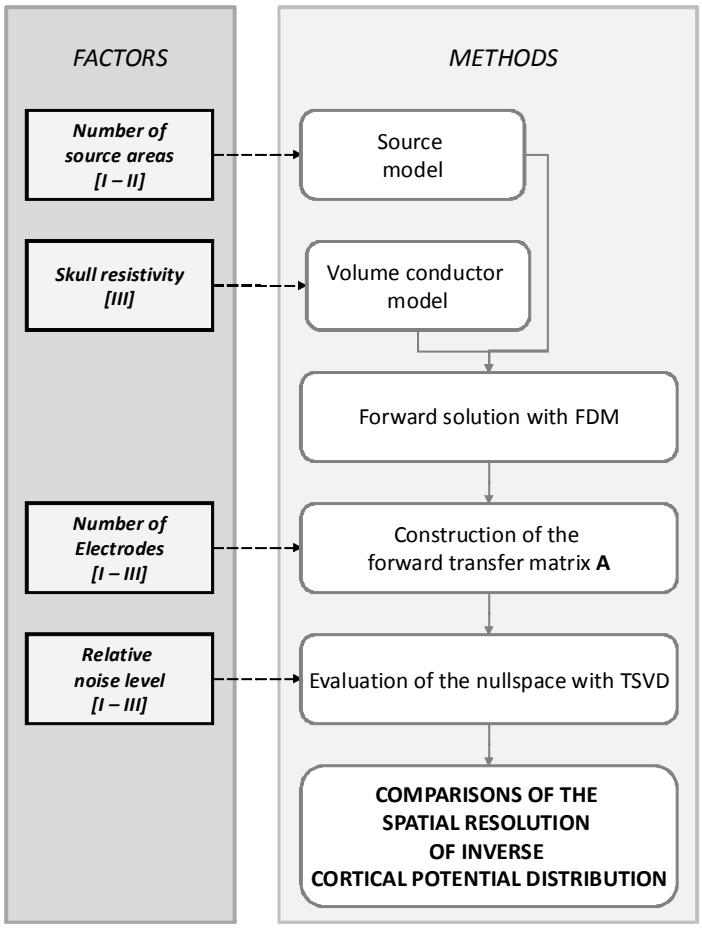


Figure 4.1. Summary of the analysis of the spatial resolution of cortical potential distribution with TSVD. The factors affecting the spatial resolution are given in the left column and they are linked to the corresponding steps in the methods given in the right column.

## 4.4 Improved signal quality of deep EEG sources [IV-VII]

### *4.4.1 Synthesisation of multielectrode EEG leads*

Multielectrode EEG leads were studied to improve the SNR of signals generated by deep EEG sources. The development of weighted multielectrode EEG leads has its basis in the

synthesisation of an optimal measurement sensitivity distribution for deep sources. Sensitivity distributions within the brain volume were calculated with the analytical equations derived by Rush and Driscoll (1969).

In [VI] and [VII] the interest focused on synthesising an optimal sensitivity distribution for deep EEG sources. According to the reciprocity theorem, the sensitivity is proportional to the distribution of the reciprocal current, and thus it can be concluded that with scalp electrodes it is impossible to obtain such a sensitivity distribution which is concentrated at the centre of the volume conductor. It was assumed that the best sensitivity distribution realized for deep sources is the uniform sensitivity distribution. Thus the lead fields of multielectrode leads were modified in a way that the sensitivity distributions were as uniform as possible within the brain volume. In [VI] the equation for calculating the weights was derived for the three-layer spherical head model. The calculation of the weights is based on the locations of the electrodes and they are incrementally proportional to:

$$w \propto \cos\theta \cos\phi \tag{4.1}$$

In Figure 4.2. an electrode is illustrated with a black dot. It is considered to lie on the circumference of a disk parallel to the xz-plane, as illustrated by the grey line in (a). In (b) the disk is plotted on the xz-plane and $\theta$ is the angular displacement of the electrode location from the negative z-axis. In (c) the disk is illustrated on the xy-plane and $\phi$ is the angular displacement of the disk from the x-axis. Now when the weights for uniformly distributed electrodes are calculated with Equation (4.2), the uniform lead field will be oriented along the positive z-axis.

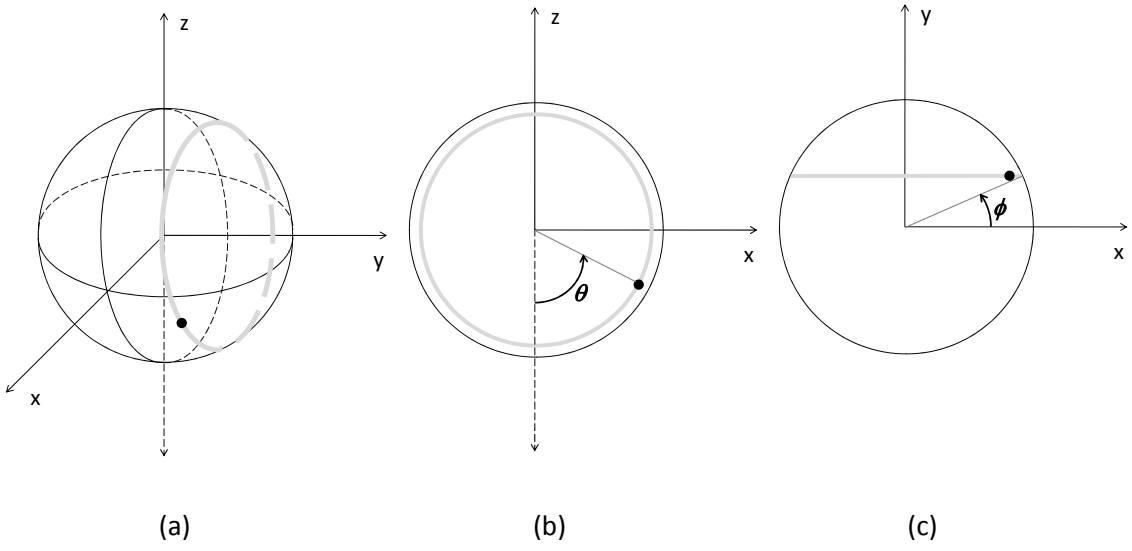


Figure 4.2. Coordinate system for the spherical head model. Black dot represents an electrode. (a) a 3D-presentation of a sphere, grey line represents the circumference of a disk parallel to xz-plane, where the electrode is located. (b) projection on the xz-plane, $\theta$ is the angular displacement of the electrode location from the negative z-axis $\theta$. (c) projection on the xy-plane, $\phi$ is the angular displacement of the disk from the x-axis.

### 4.4.2 Sensitivity distribution analysis

For the analysis of the properties of sensitivity distributions a new parameter called region of interest sensitivity ratio (ROISR) was developed and introduced in [IV]. ROISR is defined as the average magnitude of the sensitivity within the region of interest divided by the average magnitude of the sensitivity within the rest of the source volume (nonROI):

$$ROISR = \frac{\frac{1}{V_{ROI}} \int_{V_{ROI}} \left\| \mathbf{J}_L \right\| dv}{\frac{1}{V_{nonROI}} \int_{V_{nonROI}} \left\| \mathbf{J}_L \right\| dv} \tag{4.2}$$

ROISR parameter defines how well the measurement sensitivity is concentrated within the ROI. In [VI] a second parameter called nonROIsd was introduced to further analyze the properties of sensitivity distributions. The nonROIsd describes the uniformity of the magnitude of the sensitivity within the nonROI volume. It is calculated as the standard deviation of the magnitude of the sensitivity within nonROI divided by the average magnitude of the sensitivity within nonROI.

The ROISR parameter was also applied in the analysis on the specificity of bipolar EEG leads to sources located at different depths within the brain in [IV] and [V]. In [IV] the correlation between the ROISR and SNR of visual evoked potentials (VEP) was evaluated.

### 4.4.3 Simulation study

In [VI] a simulation study was conducted to compare the properties of multielectrode leads and bipolar leads. The effect of the number of electrodes in a multielectrode lead and also the effect of electrode distribution was evaluated. In the simulation study all the noise components were simulated with uncorrelated Gaussian white noise (GWN). The noise-contaminated signal $x(t)$ of the multielectrode lead can be calculated with

$$x(t) = \sum_{i=1}^{L} w_i \left[ s_i(t) + n_i(t) \right] , \tag{4.3}$$

where $w_i$ is the weight of unipolar lead $i$, $s_i$ is the signal measured with unipolar lead $i$, $n_i$ is the noise in unipolar lead $i$ and $L$ the number of unipolar leads from which the multielectrode lead is synthesized. The signals $s_i$ were calculated with Equation (3.10), and GWN was added to these calculated signals.

### 4.4.4 Experimental measurements

In [IV], the correlation between the ROISR and SNR of two-electrode leads was evaluated with an experimental measurement. For this purpose VEPs evoked by checkerboard stimulation (Celesia *et al.* 1993) were measured with a 256-channel EEG cap.

In [VII] the multielectrode lead method was validated with preliminary experimental measurements. BAEPs, generated in the auditory pathway passing through the cochlear nerve, pons and midbrain, were chosen as the EEG data. In the analysis, the BAEP components generated in the pons and midbrain were considered. The test subjects were four volunteers (3 male, 1 female, mean age 28) with normal BAEP. The EEG data was recorded as unipolar channels with a 124-channel EEG cap. For the calculation of the lead fields the digitized electrode coordinates were fitted on the surface of a three-layer spherical head model. The fitting was done by first re-centring the electrode coordinates in a way that they best fitted the spherical surface. The re-centring was done with functions found in EEGLAB (Delorme and Makeig 2004). The signals of the synthesized multielectrode leads were calculated with Equation (4.3), where the recorded signal of each unipolar lead is $s_i(t) + n_i(t)$. SNRs of synthesized multielectrode leads and also of traditionally applied bipolar BAEP leads were calculated to investigate the benefits obtained with the weighted multielectrode EEG leads. For the calculation of the amplitude SNRs in [IV] and [VII] the equations adopted from Raz *et al.* (1988) were applied.

# 5 RESULTS

## 5.1 Spatial resolution of cortical potential distribution

### *5.1.1 Effect of measurement noise*

The effect of measurement noise on the spatial resolution of cortical potential distribution was evaluated by plotting the $\sigma_i/\sigma_1$ -curves for different forward transfer matrices [I-III]. In Figure 5.1 the $\sigma_i/\sigma_1$ –curves are plotted for different resistivity ratios between scalp, skull and brain and for different electrode systems. The maximal index *i* of the source basis vectors that can be reconstructed was estimated according to Equation (3.9).

In Figure 5.1 the number of cortical source areas is 8450. In [I - II] the effect of the number of cortical source areas was also investigated as the number of source areas varied between 52 and 8450. When the number of reconstructable basis vectors (RBVs) was evaluated as a function of the number of source areas (e.g., Figure 3, in [I]), it was observed that as the number of source areas was increased from 2000 to 8450, the number of RBVs for each system was almost constant. The same phenomenon was observed for other relative skull resistivity values. Thus the division of the cortical surface into 8450 source areas does not limit the result obtained regarding the number of reconstructable basis vectors.

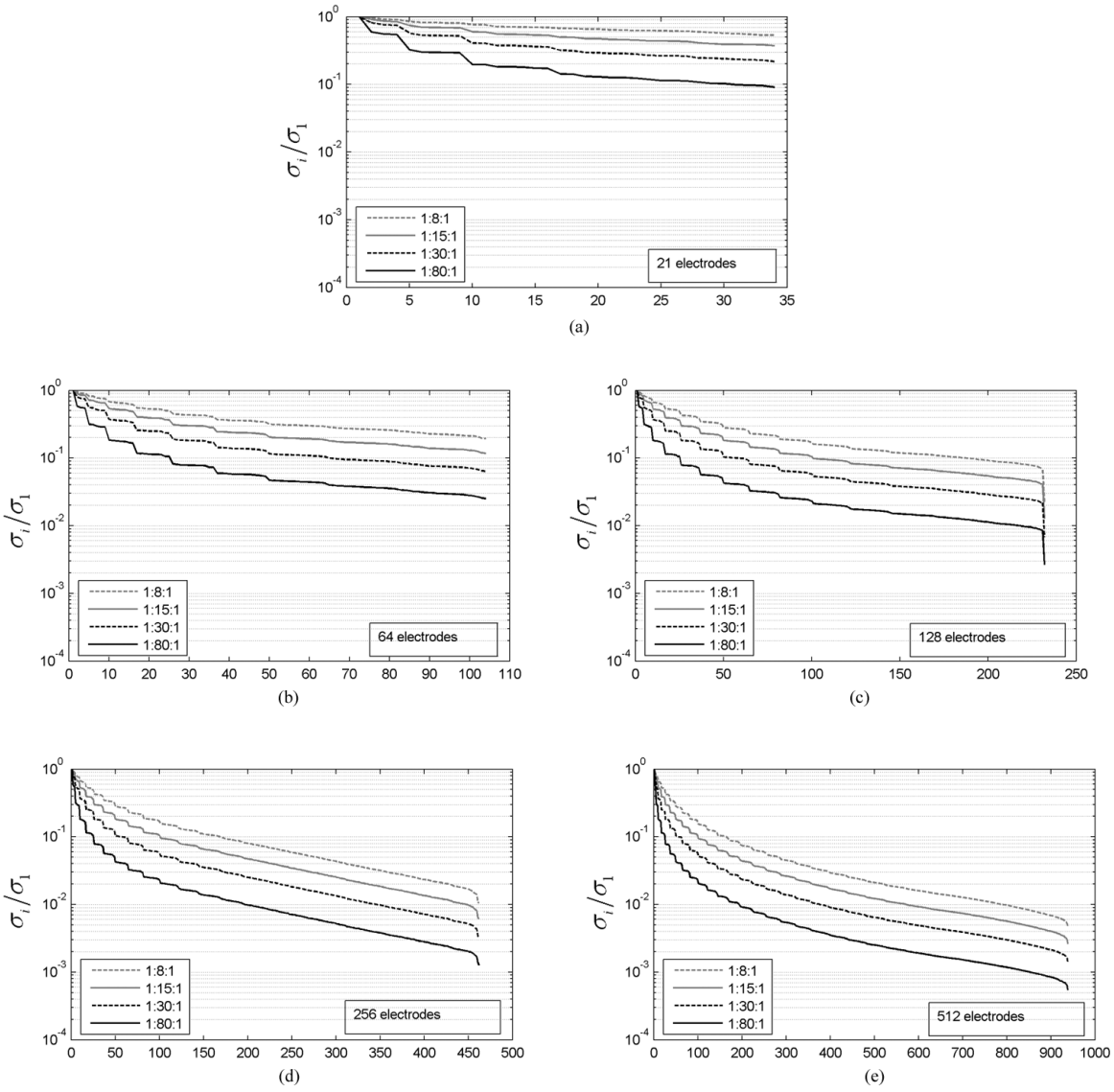


Figure 5.1. Normalized singular values $\sigma_i/\sigma_1$ sketched for different resistivity ratios for scalp, skull and brain. In (a)–(e) the numbers of electrodes on the whole spherical surface are 34, 104, 232, 462, and 938, respectively. These correspond to existing electrode systems of 21, 64, 128, 256, and 512 electrodes, respectively. [III]

### *5.1.2 Estimation of the relative noise level*

In [I] relative noise levels 0.001, 0.005, 0.05 and 0.1 were studied. These values were adopted from the literature on ECG (Dössel *et al.* 1998; Schneider *et al.* 1998) and EEG studies (Wang and He 1998). In [II] the objective was to estimate realistic noise levels present when solving the inverse cortical potential distribution.

In the knee measurements the rms noise varied between 1.6 and 3.5 µV. When the data was low-pass filtered below 30 Hz, the minimum noise voltage was 1.5 µV. In the anaesthesia data, the rms noise during suppression varied between 1.4 and 4.0 µV. When the data was low-pass filtered below 30 Hz, the minimum noise voltage was 1.1 µV. [II]

The EEG amplitude values are given in peak-to-peak values in the literature (Niedermeyer 2005a). In Table 2 of [II] the peak-to-peak amplitudes were erroneously considered as amplitude values and the rms values were calculated from these values. Taking this error into account, the relative noise levels are recalculated in Table 5.1. EEG rms amplitude of 40 µV mentioned in [I] was obtained during spontaneous brain activity. This value is also given in the Table 5.1.

Table 5.1 Relative noise levels for typical EEG amplitudes and measured noise amplitudes [II].

| | **Noise level** | | | |
|---|---|---|---|---|
| EEG (µV,rms) | n = 1.1 µV | n = 1.4 µV | n = 2.0 µV | n = 4.0 µV |
| 7.07 | 0.156 | 0.198 | 0.283 | 0.566 |
| 17.68 | 0.062 | 0.079 | 0.113 | 0.226 |
| 24.75 | 0.044 | 0.057 | 0.081 | 0.162 |
| 35.35 | 0.031 | 0.040 | 0.057 | 0.113 |
| 40 | 0.028 | 0.035 | 0.050 | 0.100 |
| 70.71 | 0.016 | 0.020 | 0.028 | 0.057 |
| 106.07 | 0.010 | 0.013 | 0.019 | 0.038 |

### *5.1.3 Effect of skull resistivity on the spatial resolution of cortical potential distribution*

The effect of skull resistivity on the spatial resolution is illustrated in Figure 5.1. When the plots for all electrode systems are evaluated it can be observed, as expected, that the higher the relative skull resistivity is, the more sensitive the spatial resolution is to measurement noise.

The spatial resolution of the 10-20 system is mainly limited by the small number of electrodes and less so by the amount of measurement noise. Regardless of the skull resistivity, the relative noise level can be over 10 % before the measurement noise starts to limit the spatial resolution. However, with dense electrode systems the measurement noise is a critical limiting factor in the inverse solution. As the noise increases, the spatial resolution decreases considerably.

Regardless of the skull resistivity the spatial resolution of a 512-electrode system is already limited by noise when the relative noise level is 0.05 %. This noise level is lower than any realistic noise level in EEG measurements, and thus the spatial resolution of a 512 electrode system is in all cases limited by the measurement noise. Moreover, when considering the 256 electrode system, regardless of the skull resistivity, with relative noise levels over 2 %, the spatial resolution is limited by the measurement noise.

In [III] it was assumed that, if with a certain electrode system at least 10 % more basis vectors can be reconstructed than with other electrode systems, then better spatial resolution can be obtained with this particular electrode system. With this criterion, those relative noise levels were evaluated at which a certain denser electrode system provides better spatial resolution than sparser electrode systems. The resulting relative noise levels are listed in Table 5.2.

Table 5.2 Relative noise levels for optimal electrode systems [III].

| RELATIVE NOISE LEVELS FOR OPTIMAL ELECTRODE SYSTEMS | | | | | |
|---|---|---|---|---|---|
| | | scalp : skull : brain–resistivity ratio | | | |
| | | 1:8:1 | 1:15:1 | 1:30:1 | 1:80:1 |
| optimal electrode system | 64 electrodes | < 37 % | < 24 % | < 15 % | < 5.9 % |
| | 128 electrodes | < 15 % | < 9.2 % | < 5.0 % | < 2.0 % |
| | 256 electrodes | < 5.7 % | < 3.4 % | < 1.8 % | < 0.69 % |
| | 512 electrodes | < 3.1 % | < 1.6 % | < 0.92 % | < 0.35 % |

## 5.2 Improved signal quality of deep EEG sources

### *5.2.1 ROISR parameter in defining the specificity of an EEG lead*

In the analysis of different leads with the introduced ROISR parameter, it was found that the specificity of different leads was affected by the depth of the ROI, the relative skull resistivity and the number of electrodes in the lead [IV - VI].

In [IV] the correlation between ROISR and SNR of several EEG leads was studied. The EEG data was obtained by measuring visual evoked responses with a 256-channel EEG cap. The results show that if the ROI volume is properly selected, the ROISR has a high correlation to the SNR of the lead. In two cases studied, the correlations were 75 % and 92 % (not 82 % and 94 % as erroneously stated in [IV]).

### *5.2.2 Effect of source depth on the specificity of two-electrode EEG leads*

ROISR analysis was conducted to evaluate the optimal electrode distance for two-electrode leads when the region of interest is located at different depths [V]. For the sources located at the centre of a three-layer model, i.e., close to the pons and midbrain, the optimal electrode distance is 180°. In addition, the closer the ROI is located to the surface of the brain, the smaller is the optimal electrode distance; this was as expected. The relative skull resistivity affects the optimal electrode distance for intermediate ROI depths 4 – 6 cm below the cortical surface. For cortical ROIs the placement of electrodes needs to be considered carefully because a small change in the electrode distance can considerably reduce the specificity [V].

### *5.2.3 Specificity of a multielectrode EEG leads for deep EEG sources*

The specificity of multielectrode leads was studied with the ROISR and nonROIsd parameters. If the electrodes are uniformly distributed on the surface of the three-layer spherical head model as in the studied theoretical multielectrode leads, the uniform sensitivity distribution can be obtained when the weights for unipolar leads are calculated according to Equation (4.1) [VI]. In Figure 5.2 the sensitivity distribution of a theoretical multielectrode lead consisting of 102 electrodes is illustrated. The placement of the electrodes uniformly over the scalp surface is unrealistic in experimental EEG

measurements, and thus the specificity of more realistic electrode systems was also studied. The electrode coordinates of a 124-channel EEG cap were fitted on the surface of a three-layer spherical head model. A disadvantage of Neuroscan caps, at least, is that they cover only the upper part of the scalp surface and thus with the present experimental multielectrode leads it is not possible to obtain uniform sensitivity distributions [VI-VII]. Figure 5.3 gives an example of a sensitivity distribution of an experimental multielectrode lead consisting of 115 electrodes.

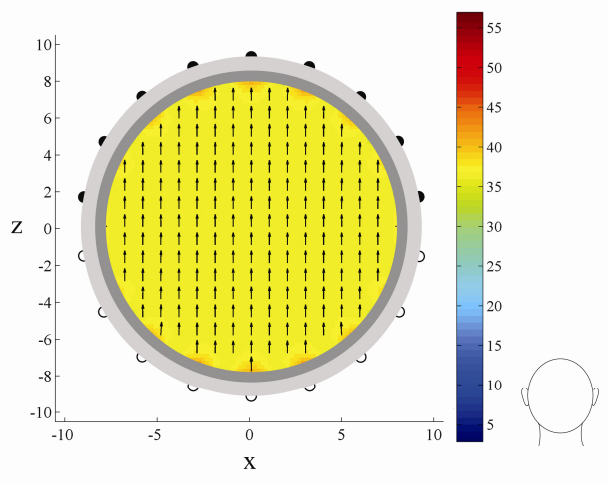


Figure 5.2. Sensitivity distribution of a theoretical multielectrode lead consisting of uniformly distributed 102 electrodes. Sensitivity distribution is illustrated with lead vectors within the brain volume on the xz-plane (y=0). The colour scale gives the magnitude of sensitivity distribution in $A/m^2$. [VI]

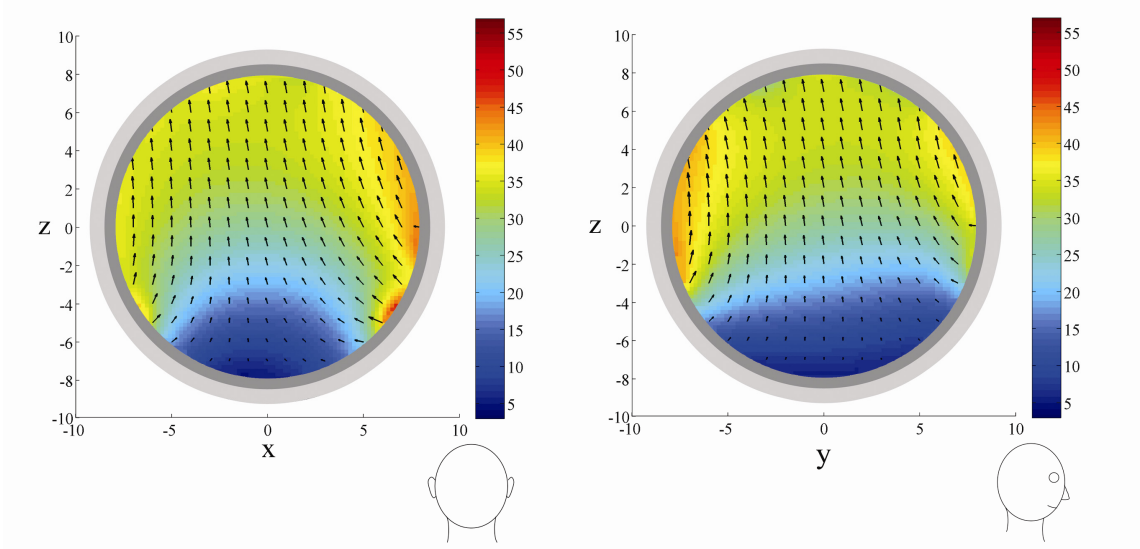


(a) (b)

Figure 5.3 Sensitivity distribution of an experimental multielectrode lead consisting of 115 electrodes. Sensitivity distributions are illustrated with lead vectors within the brain volume on the a) xz-plane (y=0) and b)yz-plane (x=0). The colour scale gives the magnitude of sensitivity distribution in $A/m^2$. [VI,VII]

When the sensitivity distributions were analysed with the developed parameters, the specificity of the experimental multielectrode leads was improved in comparison with the two-electrode leads. However, it was not as good as with the theoretical multielectrode leads [VI]. The average number of electrodes in the eight experimental multielectrode leads that were studied was 114. When 102 electrodes were uniformly distributed on the scalp surface the ROISR was 1.00 and nonROIsd 0.93 %, whereas in the experimental multielectrode leads, the ROISR was on average 0.953 and the nonROIsd 30.1 %.

### *5.2.4 Improvement in SNR in a simulation study*

The simulation results obtained on the improvement of SNR corresponded to the results obtained by studying the specificity of different leads [VI]. Simulation studies were conducted both with two-electrode leads and with multielectrode leads. As expected, with two-electrode leads the highest SNR was obtained when the electrode distance was 180°.

In theoretical multielectrode leads the SNR was dependant on the number of electrodes. This was anticipated because the noise was modelled with GWN. When the SNR improvement obtained with temporal averaging is compared to SNR improvement obtained through spatial averaging, it is seen that the latter is smaller than proportional to the square root of the number of unipolar leads.

The ROISR analysis showed that the theoretical multielectrode leads are more specific to deep sources than the experimental multielectrode leads. It could be assumed on the basis of the ROISR analysis that better SNR improvement would be obtained with theoretical rather than with experimental multielectrode leads with approximately the same number of electrodes. The results of the simulation study show that the SNR obtained with the theoretical multielectrode lead consisting of 102 electrodes was 1.6 times better that obtained with the experimental lead consisting on average of 114 electrodes [VI].

### *5.2.5 Experimental evaluation of multielectrode EEG leads*

Experimental BAEP measurements conducted with a 124-channel EEG cap confirmed the improvement in SNR obtained with multielectrode EEG leads [VII]. SNRs were evaluated separately for two time intervals. The first interval included the BAEP peaks I-V. During this time interval the activation proceeds from the eighth cranial nerve through the medulla and pons up to inferior colliculus in the midbrain (Scherg and von Cramon 1985; Nuwer *et al.* 1994; Chiappa and Hill 1997; Celesia and Brigell 2005). The orientation of the signal source also changes during this time interval from horizontal to vertical (Scherg and von Cramon 1985). The second studied time interval included the peaks IV-V, during which the source orientation is almost vertical (Scherg and von Cramon 1985). The SNRs were calculated for traditional BAEP channels Cz-Ai and Cz-Ac. In some cases the Cz referred to a neck electrode gave higher SNR than either of the traditional leads (Nuwer *et al.* 1994).

During peaks I-V, the SNR obtained with a multielectrode lead was 1.4 – 1.9 times greater than that of either of the traditional BAEP leads. The average SNR improvement was 1.6. During peaks IV-V, the SNR obtained with a multielectrode lead was 1.2 – 1.6 times greater than that of any of the bipolar BAEP leads studied. The average SNR improvement was 1.5 [VII].

For the comparison of the experimental data and the simulation data, the SNR of the traditional BAEP lead Cz - Ai was compared to the SNR of the multielectrode lead during the peaks IV-V. In the case of the experimental data, the SNR obtained with a multielectrode lead was on average 1.7 ($\pm$0.24) times greater than that of a bipolar lead. In the simulation study conducted with the same leads, the SNR of multielectrode leads was on average 2.3 ($\pm$ 0.16) times greater than that of bipolar lead. [VI]

# 6 DISCUSSION

## 6.1 Multichannel EEG

The purpose of this thesis is to investigate how multichannel EEG can be applied to improve the accuracy of EEG measurements. This question was addressed using two different approaches. The first approach investigated how the increase in the number of measurement electrodes improves the spatial resolution of the cortical potential distribution. The second approach sought to improve the signal quality of the other extreme of EEG sources; the deep sources located in the brainstem.

The results on the improvement of the spatial resolution of inverse cortical potential distribution show that with current knowledge of relative skull resistivity, the increase of measurement electrodes up to 256 increases the spatial information content of the inverse cortical potential distribution that can be solved from the scalp potential data.

When considering the registration accuracy of the signals generated by the deep EEG sources, the first step is to synthesize a more specific sensitivity distribution than that of traditional two-electrode leads. Application of a high number of electrodes in a multielectrode lead enables the synthesis of more specific sensitivity distributions for deep sources. A major advantage of applying multichannel EEG is the possibility to easily orientate the sensitivity distribution parallel to the source orientation. When recording EEG with a multielectrode lead, the spatial averaging that results from the application of a high number of measurement electrodes further improves the SNR of the signals generated by deep EEG sources.

## 6.2 Spatial resolution of cortical potential distribution

### *6.2.1 Measurement noise*

Measurement noise was one of the factors whose effect on the spatial resolution of the cortical potential distribution was studied. The amount of the measurement noise has a substantial effect on the accuracy of the inverse solution. Because the inverse problem is highly ill-conditioned, especially when a large number of electrodes are used, the effect of noise needs to be carefully considered (Michel *et al.* 2004). All of the systems studied in [I

- III] were highly ill-conditioned; the larger the number of electrodes and the higher the relative skull resistivity is, the more ill-conditioned the inverse problem is.

Typical relative noise levels were approximated by investigating the amplitudes of EEG signals and noise signals [I, II]. It is impossible to completely suppress the noise because there always exists at least the noise components resulting from electrode noise and instrumentation noise. With electrically shielded rooms, the effect of environmental noise can be reduced to a minimum and by instructing the patient, the effect of other biological noise components can also be greatly reduced.

The results showed that the measurement noise can be reduced to a level of 1 – 4 $\mu V_{rms}$. These values agree with the reported values for electrode interface noise (Fernandez and Pallas-Areny 2000; Huigen *et al.* 2002) and instrumentation noise (Kamp *et al.* 2005). The measurements were conducted in an unshielded laboratory, and thus these levels should be achievable in most measurement environments. The relative noise level is also clearly dependent on the amplitude of the EEG signal. With the above noise estimates and average EEG amplitude of spontaneous activity, the relative noise levels vary between 0.03 and 0.1.

The effect of measurement noise has only been reported in a few studies concerning inversely solved cortical potential distributions (Wang and He 1998; He *et al.* 1999). In both of these studies the benefits obtained with a higher number of measurement electrodes were greater than in the present thesis. In both of these studies the head was modelled as a three-layer spherical model with a relative skull resistivity of 80. Wang and He (1998) studied relative noise levels of 5 % and 10 %. The higher number of electrodes provided better accuracy regardless of the amount of noise. The application of 301 electrodes resulted in slightly higher accuracy than the 128 electrode system, though the difference was insignificant. He *et al.* (1999) studied relative noise level of 5 % and the accuracy they obtained with 310 electrodes was clearly better than that obtained with 128 electrodes.

Based on the results of this thesis, the relative noise level would need to be below 0.69 % for the 256 electrode system to give better spatial resolution than the 128 electrode system. This value is much lower than the actual noise levels in spontaneous EEG recordings. The major difference between other studies and the present is that here no sources were simulated, but the accuracy of the inverse solution was evaluated solely on the basis of the properties of the forward transfer matrix. Wang and He (1998) and He *et al.* (1999), for example, modelled the source distribution by placing two dipolar sources within the brain.

### *6.2.2 Relative skull resistivity*

A wide variety of the skull resistivity values have been reported in the literature, and numerous resistivity ratios have been suggested between the different tissues in the head models. The earliest resistivity ratio 1:80:1, suggested by Rush and Driscoll (1968) can be fairly discarded because it resulted from estimations made with a post mortem skull sample. However, it does provide an indication for a value to be applied in three-layer

spherical head models because Rush and Driscoll optimized this value between the realistically shaped tank model and an analytical three-layer spherical head model. If more recent information regarding the ratio between live and post mortem skull samples is considered, the Rush and Driscoll estimate of the relative skull resistivity could be updated to be between 27 and 40.

The newer estimates for the relative skull resistivity in three-layer spherical head models have varied between 25 and 72 (Goncalves *et al.* 2003a; Lai *et al.* 2005), and in realistically shaped three-layer models between 15 and 50 (Oostendorp *et al.* 2000; Goncalves *et al.* 2003b; Zhang *et al.* 2006b). The relative skull resistivity values suggested on the basis of the measurements of skull samples indicate values between 8 and 18 (Oostendorp *et al.* 2000; Akhtari *et al.* 2002; Hoekema *et al.* 2003). Nunez and Srinivasan (2006) reported that in three-layer models a higher value for skull resistivity should be applied than in four-layer models. If this result is kept in mind while examining the reported skull resistivity values, it could be approximated that the relative skull resistivity in three-layer spherical head models is at minimum between 15 and 30. It should also be noted that relative skull resistivity increases with age and that there are also interindividual variations.

### *6.2.3 Electrode density*

An essential question is how many electrodes should be applied on the surface of the scalp to improve the spatial resolution of EEG. Many different factors affect to the appropriate number of electrodes, the most important being the amount of measurement noise. Thus, for different EEG measurements conducted in different environments, the appropriate number of electrodes may vary considerably. Clearly in any measurement such noise levels are obtainable, that justify using at least 64 measurement electrodes to improve the spatial resolution. In this thesis it was estimated that while measuring spontaneous activity, noise levels of 3 % are achievable. This would suggest than if the relative skull resistivity is 15, then 256 electrodes still improve the spatial resolution. If, on the other hand, the relative skull resistivity is closer to 30, then 128 electrodes would be sufficient.

The estimates on the relative noise levels in this thesis were calculated on the basis of spontaneous EEG data. When the purpose is to solve the cortical potential distribution of evoked potentials, averaging of several epochs can be applied to improve the SNR and thus to lower the noise level. Even though the amplitudes of evoked potentials are typically lower than those of spontaneous activity, lower noise levels might be achievable in evoked potential measurements than in spontaneous measurements. Babiloni *et al.* (1997b) have reported noise levels below 5 % in EP measurements when special attention was paid to lowering the noise components in the measurement. The introduction of active electrodes to EEG measurements might further reduce the noise levels. If 1% noise levels are possible to obtain by averaging, then the application of even 512 or 256 electrodes would result in improved accuracy of the cortical potential distribution in the case of 15 and 30 relative skull resistivity, respectively.

### 6.2.4 TSVD in defining spatial resolution

The TSVD-based method applied in this thesis is a convenient method to study the effect of measurement noise on the accuracy of the inverse solution. An important property of the method is that only a forward transfer matrix of the source-field relationship is needed. The method gives a rough estimate of the number of basis vectors that can be reconstructed, but the benefit is that the results are not confined to certain source distribution patterns.

Naturally the complexity of the cortical potential distribution affects the amount of regularization needed. For example, the cortical potential distributions generated by deep sources have low spatial frequency, and thus more regularization can be applied without reducing the spatial resolution (Wang and He 1998). The reason for this is that the source basis vectors $\mathbf{v}_i$ tend to have more sign changes with growing index $i$, and thus the truncation of small singular values does not affect low spatial frequencies (Hansen 1998). When the purpose is to estimate the maximal spatial resolution, the most complex potential distribution patterns requiring the highest amount of regularization should be considered.

The TSVD has also been applied by Wang and He (1998) and Babiloni *et al.* (1997b) as a regularization method in CIT studies. In both of these studies simulations were conducted, and thus the "true" solution of the cortical potential distribution was available for comparison. Babiloni *et al.* (1997b) concluded that an amount of 5 % or 10 % noise did not affect the regularization parameter, but it still reduced the correspondence between predicted and simulated potentials. Wang and He (1998) evaluated the optimal value of "noise ratio" for simulated data to which a different amount of measurement noise was added. Their definition of noise ratio is the same as the definition of noise level in Equation (3.9). They evaluated the optimal value of the noise ratio for dipolar sources with different eccentricity. Of interest are the results for the most superficial sources. Their results showed that for superficial sources, the optimal noise ratio is lower than the noise level of the data. Thus their results suggest that more basis vectors could be reconstructed than calculated on the basis of Equation (3.9) of this thesis. Thus in the future studies it would be interesting to investigate cortical potential distribution with different spatial frequency spectra in order to evaluate the accuracy of Equation (3.9).

### 6.2.5 Accuracy of the applied models

In the present thesis a three-layer spherical head model was applied as a volume conductor model. The largest modelling errors in spherical head models concern the skull. As can be seen from Figure 3.4, the centre of a three-layer spherical head model can be so adjusted that it represents an actual anatomical region. A spherical head model was selected because the purpose was to evaluate the effect of measurement noise and relative skull resistivity on the accuracy of the cortical potential distribution. Thus a model was selected that is not bound to any particular head geometry. In future studies, for example, realistically shaped generic head models could be applied to adjust the estimates of the spatial resolution of high-resolution EEG (Darvas *et al.* 2006).

## 6.3 Improved signal quality of deep EEG sources

### *6.3.1 Specificity of EEG leads*

The ROISR parameter introduced here provides a convenient way to estimate the relative sensitivity of different leads to sources in predefined areas through modelling. The correlation between the ROISR and SNR of two-electrode leads was studied in a preliminary experimental test and it was shown that for superficial sources a high correlation exists. In the simulation study and in experimental evaluation of the multielectrode leads, both the SNRs and ROISRs were calculated for bipolar and multielectrode leads. The improvement in SNR was markedly higher than could have been anticipated on the basis of the ROISR values alone. Thus it was concluded that spatial averaging of the noise also occurs when several electrodes are applied in the synthesisation of a multielectrode lead. Spatial averaging is not only a property of multielectrode leads, but can also be applied in other multichannel measurements to improve the SNR as described in section 3.1.5.

With the ROISR parameter introduced here, the optimal electrode distance in a two-electrode lead for sources located at different depths was also evaluated [VI]. It could be questioned whether all of these different depths have practical relevance. A large population of neurons needs to be active synchronously for a potential difference to be measurable on the surface of the scalp. Moreover, the organization of the neurons needs to be such, that the magnitude of the dipole moment is increased through superposition. Although the structure of the cerebral cortex varies from region to region (Crossman and Neary 2000), it generally has an organization that can generate measurable potentials. Because of the folded structure of the cerebral cortex, some cortical generators lie relatively far from the scalp surface. Especially the large fissures, such as the great longitudinal fissure and the Sylvian fissure, extend fairly deep. For example, the primary auditory cortex is located in the Sylvian fissure and the somatosensory and motor areas represented by the lower limbs are located on the medial surfaces of the hemispheres, deep in the great longitudinal fissure above the corpus callosum (Crossman and Neary 2000). Brainstem-evoked potentials can be measured from the surface of the scalp, and as illustrated in Figure 3.4, the brainstem and midbrain are located close to the centre of a three-layer spherical head model. In future studies the effect of the realistic shape of the head model should be evaluated when studying these deeper source locations.

### *6.3.2 Spatial averaging in multielectrode EEG leads*

In the multielectrode lead analysis, GWN was added to the signals measured from the surface of the scalp. This noise signal was used to model all the noise components of biological and technical origin. As was shown, for example, by Srinivasan *et al.* (2007), even the uncorrelated background EEG measured from moderately separated surface electrodes is correlated because of the volume conductor effects. In the frequency band which is used to measure brainstem evoked potentials, the background EEG might be uncorrelated. However, because of the shown volume conductor effects, the spatial averaging in real measurements is not as efficient as in the conducted simulation.

How the increase in the electrode number affects the SNR of multielectrode leads has not so far been evaluated here. Thus in future studies, the effect of spatial averaging should be studied as a function of the electrode distance in order to determine the appropriate number of electrodes to be included in the multielectrode lead. Even though the correlation of background EEG reduces the effect of spatial averaging as the number of electrodes is increased, there are still benefits in applying a large number of electrodes, preferably distributed as broadly over the scalp surface as possible. The advantage is due to the fact that the measurement sensitivity is easier to orientate in order to be parallel to the source dipole. This is a natural goal in any EEG measurement because it maximizes the signal amplitude.

### *6.3.3 Feasibility of multielectrode EEG leads*

A present drawback of multielectrode leads is the long application time needed to prepare the electrode contacts. This time is considerably more than that saved with shorter recording time. New technologies, such as active electrodes, will be applied in the future to overcome this drawback. Active electrodes have been studied for forty years, and recently new active electrodes have been developed with a reasonable price and good construction (Metting van Rijn *et al.* 1996; Ko 1998; Degen and Jackel 2006). The main advantage of active electrodes is that they can be applied without conductive paste and abrasive skin preparation, which will shorten the electrode preparation time considerably (Ko 1998). An active electrode has high input impedance in gigaohms and low output impedance. Thus mismatches between electrode impedances are tolerated better with active rather than passive electrodes and the amount of interference coupled through electrode leads is also reduced (Ko 1998). In addition, new active electrode EEG caps, where the electrodes cover the scalp surface as comprehensively as possible, should be constructed to further develop the multielectrode lead method.

Even if the measurements are conducted with passive electrodes, a major advantage of multielectrode leads is the shorter measurement time. Fewer epochs are needed for the average to obtain a satisfactory SNR. This reduced the effects of changes in the response signal when the number of stimuli is decreased. Such changes might arise because of fatigue, learning habituation or changes in the level of alertness of the subject.

### *6.3.4 Comparison to other SNR improvement methods*

A large variety of other methods have been developed to improve the SNR of evoked potential measurement (Sörnmo and Laguna 2005). Some of these methods are applied to signals measured with a single bipolar channel. The multielectrode lead method produces as an output a single channel measurement. Thus the other methods for improving the SNR of single channel measurements can be applied in addition to the multielectrode lead method to further improve the SNR. These methods include, for example, median averaging (Özdamar and Kalayci 1999), weighted averaging (Davila and Mobin 1992), Bayesian weighted averaging (Don and Elberling 1994) trimmed estimators (Leonowicz *et al.* 2005) and sorted averaging (Mühler and von Specht 1999). The basic idea in all these methods is that in actual EEG measurements the noise across sweeps is not stationary. In the case of non-stationary noise, all these methods have been shown to

increase the SNR compared to traditional averaging. The amount of noise can be increased, for example, by muscular activity or by changes in the subject's state of relaxation (Mühler and von Specht 1999). In addition wavelet-based denoising methods have been introduced that are applied to signals measured from a single channel (Causevic *et al.* 2005).

For example, in Neuroscan software there exists a so-called Fsp Average, introduced by Elberling and Don (Elberling and Don 1984; Don and Elberling 1994). This average is especially designed for BAEP measurements. In the Fsp Average a single-point F-statistic is applied in order to evaluate the quality of the measured signal and the Bayesian weighted averaging is applied to calculate the average. The application of a multielectrode lead does not prevent the application of the Fsp average, but it can be applied in addition to the multielectrode lead to further improve the quality of the measurement.

### *6.3.5 Comparison to beamformers*

The other set of SNR improvement methods are based on the application of the data measured from a number of channels. The best known of these methods are spatial filtering methods called beamformers (Van Veen *et al.* 1997; Ward *et al.* 1999). The criterion of an optimal spatial filter is similar to the goal of the present multielectrode lead method. To completely suppress the noise generated within the brain, the magnitude of the sensitivity distribution should be zero outside the source location. As shown by the reciprocity theorem, this criterion cannot be achieved for deep EEG sources. The multielectrode lead Equation (4.3) is the same as the output equation of the beamformers (Van Veen *et al.* 1997), but the method of choosing the weights is different. In beamformer methods lead vectors are also calculated, but the selection of the spatial filter weights is made only on the basis of the lead vector at the target region and the covariance matrix of the measured signals. Optimally the beamformer output is an estimate of equivalent dipole moment of the dipole at the target location.

Ward et al. (1999), using both simulated and realistic data, investigated how the LCMV beamformer can be applied to enhance deep epileptiform data. They applied a three-layer spherical head model with a relative skull resistivity of 80. In their simulations they studied, for example, the effect of the number of measurement electrodes and eccentricity of the source on the SNR improvement obtained with the beamformer. Their basic assumption for the deep source was such, that its normalized eccentricity was 0.5. The increase in the electrode number from 4 to 16 was shown to improve the performance of the beamformer. Additionally, the different source eccentricities within the brain were studied, and it was observed that greater improvements were obtained for sources located closer to the surface of the brain.

Application of a beamformer to enhance EEG activity requires prior information on the source location. Ward et al. (1999) also evaluated the sensitivity of the beamformer to the inaccuracies in the assumed depth of the source. Their results show, that for deep sources with normalised eccentricity less than 0.3, the beamfomer is sensitive to the estimate of the depth of the source. The misspecification of the source location in the

beamformer optimization might even reduce the SNR of the output signal. This is an obvious drawback of the beamformer methods compared to the multielectrode lead method presented here. When the sensitivity distribution is uniform, as in the multielectrode lead method presented here, the lead is equally sensitive to sources located at different depths. Thus a misspecification of the deep source location does not affect the results obtained with the multielectrode lead method. In the clinical evaluation Ward *et al.* (1999) evaluated the increase in the SNR, when the beamformer output was projected on the surface of the scalp. The locations of the epileptic foci were not given in the paper, but presumably they were located more superficially than the deep brainstem sources. In addition, SNR of the original signal was relatively high. Their results showed an SNR improvement of 100 %.

It can be concluded that the beamformer methods offer an alternative to the lead field-based multielectrode lead method. The multielectrode lead method can also be considered as a spatial filtering method. A great benefit of the multielectrode lead method is its simplicity. The multielectrode lead method is also more illustrative, since the best reachable sensitivity distribution in magnitude and direction for deep sources can be visualized. In addition, the weights can be defined prior to carrying out the EEG measurement. Because of the uniform sensitivity distribution of multielectrode leads, they result in the optimal improvement for deep EEG sources, when the noise sources are uniformly distributed within the brain.

In the future studies a more extensive comparison should be performed between the beamformer and multielectrode lead methods for the sources located in the brainstem. The performance of the beamformer method for extremely noisy signals, such as BAEPs, should also be evaluated. An integration of these two methods might provide the most optimal improvement, at least in cases where the noise sources are nonuniformly distributed.

### *6.3.6 Future development of multielectrode leads*

The results of the experimental study showed that with a multielectrode lead consisting on average of 114 electrodes, it is sufficient to average 45 % of the epochs that are needed with the best possible bipolar lead. The results of the theoretical study show that further improvements can be obtained by placing the electrodes more extensively over the scalp surface.

The lead field theoretical basis of the multielectrode lead method will allow further development of the method for those sources located at different depths. If the purpose is to measure responses generated by a single dipolar source, which changes its location and orientation during the studied time course, the orientation of a single multielectrode lead can be changed as a function of time. This ensures that the sensitivity distribution at each time instant is parallel to the source orientation. The prerequisite for this approach is that there is prior information on the source location and orientation. With the multielectrode lead approach it would also be possible to measure multiple simultaneous sources. Such a situation arises, for example, when measuring later responses of evoked

potentials that have subcortical generators in both hemispheres. In this case a separate multielectrode lead could be optimized for each dipolar source.

The above two extensions of the multielectrode lead method will require further development of the technique. Firstly, the present approach to synthesize the uniform sensitivity distribution is optimal only for the deepest sources. Thus numerical optimization methods need to be studied to broaden the lead field optimization for other than deep sources. The central point to be recognised is that the optimal sensitivity distribution is always concentrated at the source location and the orientation of the sensitivity distribution is parallel to the source orientation. One obvious possibility would be to form three orthogonal multielectrode leads from the same set of unipolar channels simultaneously, as has also been suggested for beamformers (Ward *et al.* 1999).

A great concern, when considering the deep sources and the synthesisation of optimal sensitivity distributions, is the effect of the head model applied. The deep structures of the head, including, for example, the ventricles around the brain stem have a particularly clear effect on the lead field patterns. These should be investigated further when developing the multielectrode lead method.

# 7 CONCLUSIONS

The purpose of this series of studies is to investigate how the application of multichannel EEG leads can improve the registration accuracy of the electric fields in the brain when measured from the surface of the scalp. Two different applications of multichannel EEG were investigated. The main conclusions of this series of studies are as follows:

- In multichannel EEG measurements the noise is a major factor limiting the accuracy of the inverse cortical potential distribution. The effect of noise needs to be carefully considered because the inverse problem is highly ill-conditioned.

- The spatial resolution of sparse electrode systems (21 – 64 electrodes) is mostly limited by the small amount of electrodes. The noise has only a minor impact on the spatial resolution.

- The spatial resolution of dense EEG systems (128 – 512 electrodes) is extremely sensitive to measurement noise. The advantage of dense electrode systems over the sparse ones is diminished as the amount of noise increases.

- The relative skull resistivity used in the calculations has a prominent effect on the accuracy of the cortical potential distribution. With the old standard value of 80, the application of 64 electrodes is shown to be sufficient in obtaining the best possible spatial resolution. The relative skull resistivity has been shown to be much lower. With realistic estimates of 15 and 30 and with the relative noise level of 3 %, the application of at least 256 or 128 electrodes, respectively, improves the accuracy of inverse cortical potential distribution.

- The ROISR parameter, which defines the specificity of the sensitivity distribution, is a practical tool to design both two-electrode and multielectrode measurement set-ups. The ROISR has a high correlation with the SNR.

- Multielectrode EEG leads improve the SNR of signals generated by deep brainstem sources. In an optimal multielectrode lead, the sensitivity distribution is uniform within the brain volume and it is oriented parallel to the source

orientation. When a large number of electrodes are applied in the synthesis of a multielectrode lead, the sensitivity distribution is easy to orientate so that it is parallel to the source orientation.

- In a multielectrode lead both the more specific sensitivity distribution and the spatial averaging of noise improve the SNR compared to bipolar leads.
- With a multielectrode EEG lead it is possible to reduce the number of recorded epochs at least to one half compared to the bipolar leads.

# 8 References


Akhtari M, Bryant HC, Mamelak AN, Heller L, Shih JJ, Mandelkern M, Matlachov A, Ranken DM, Best ED, and Sutherling WW. Conductivities of three-layer human skull. *Brain Topography*, vol. 13, no. 1, pp. 29-42, 2000.

Akhtari M, Bryant HC, Mamelak AN, Flynn ER, Heller L, Shih JJ, Mandelkern M, Matlachov A, Ranken DM, Best ED, DiMauro MA, Lee RR, and Sutherling WW. Conductivities of three-layer live human skull. *Brain Topography*, vol. 14, no. 3, pp. 151-167, 2002.

American Electroencephalographic Society guidelines for standard electrode position nomenclature. *Journal of Clinical Neurophysiology*, vol. 8, no. 2, pp. 200-202, 1991.

Babiloni F, Babiloni C, Fattorini L, Carducci F, Onorati P, and Urbano A. Performances of surface Laplacian estimators: a study of simulated and real scalp potential distributions. *Brain Topography*, vol. 8, no. 1, pp. 35-45, 1995.

Babiloni F, Babiloni C, Carducci F, Fattorini L, Onorati P, and Urbano A. Spline Laplacian estimate of EEG potentials over a realistic magnetic resonance-constructed scalp surface model. *Electroencephalography and Clinical Neurophysiology*, vol. 98, no. 4, pp. 363-373, 1996.

Babiloni F, Babiloni C, Carducci F, Del Gaudio M, Onorati P, and Urbano A. A high resolution EEG method based on the correction of the surface Laplacian estimate for the subject's variable scalp thickness. *Electroencephalography and Clinical Neurophysiology*, vol. 103, no. 4, pp. 486-492, 1997a.

Babiloni F, Babiloni C, Carducci F, Fattorini L, Anello C, Onorati P, and Urbano A. High resolution EEG: a new model-dependent spatial deblurring method using a realistically-shaped MR-constructed subject's head model. *Electroencephalography and Clinical Neurophysiology*, vol. 102, no. 2, pp. 69-80, 1997b.

Babiloni F, Carducci F, Babiloni C, and Urbano A. Improved realistic Laplacian estimate of highly-sampled EEG potentials by regularization techniques. *Electroencephalography and Clinical Neurophysiology*, vol. 106, no. 4, pp. 336-343, 1998.

Babiloni F, Carducci F, Cincotti F, Del Gratta C, Pizzella V, Romani GL, Rossini PM, Tecchio F, and Babiloni C. Linear inverse source estimate of combined EEG and MEG data related to voluntary movements. *Human Brain Mapping*, vol. 14, no. 4, pp. 197-209, 2001a.

Babiloni F, Cincotti F, Carducci F, Rossini PM, and Babiloni C. Spatial enhancement of EEG data by surface Laplacian estimation: the use of magnetic resonance imaging-based head models. *Clinical Neurophysiology*, vol. 112, no. 5, pp. 724-727, 2001b.

Babiloni F, Babiloni C, Carducci F, Cincotti F, and Rossini PM. 'The stone of madness' and the search for the cortical sources of brain diseases with non-invasive EEG techniques. *Clinical Neurophysiology*, vol. 114, no. 10, pp. 1775-1780, 2003.

Babiloni F, Babiloni C, Carducci F, Romani GL, Rossini PM, Angelone LM, and Cincotti F. Multimodal integration of EEG and MEG data: a simulation study with variable signal-to-noise ratio and number of sensors. *Human Brain Mapping*, vol. 22, no. 1, pp. 52-62, 2004.

Barr RC, Ramsey M, 3rd, and Spach MS. Relating epicardial to body surface potential distributions by means of transfer coefficients based on geometry measurements. *IEEE Transactions on Biomedical Engineering*, vol. 24, no. 1, pp. 1-11, 1977.

Berger H. Über das Elektrenenkephalogramm des Menschen. *Archiv für Psychiatrie und Nervenkrankheiten*, vol. 87, pp. 527-570, 1929.

Bradshaw LA, Wijesinghe RS, and Wikswo JP, Jr. Spatial filter approach for comparison of the forward and inverse problems of electroencephalography and magnetoencephalography. *Annals of Biomedical Engineering*, vol. 29, no. 3, pp. 214-226, 2001.

Brody DA. A method for applying approximately ideal lead connections to homogeneous volume conductors of irregular shape. *American Heart Journal*, vol. 53, no. 2, pp. 174-182, 1957.

Burger HC and Van Milaan JB. Heart vector and leads. *British Heart Journal*, vol. 8, no. 3, pp. 157-161, 1946.

Burger HC and Van Milaan JB. Heart vector and leads. Part II. *British Heart Journal*, vol. 9, no. 3, pp. 154-160, 1947.

Burger HC and Van Milaan JB. Heart vector and leads. Part III geometrical representation. *British Heart Journal*, vol. 10, no. 4, pp. 229-233, 1948.

Caton R. The electric currents of the brain. *British Medical Journal*, vol. 2, pp. 278, 1875.

Causevic E, Morley RE, Wickerhauser MV, and Jacquin AE. Fast wavelet estimation of weak biosignals. *IEEE Transactions on Biomedical Engineering*, vol. 52, no. 6, pp. 1021-1032, 2005.

Celesia G and Brigell M. Auditory evoked potentials. In *Electroencephalography: basic principles, clinical application, and related fields*, E. Niedermeyer and F. Lopez da Silva, Eds., 5th ed. Philadelphia, PA, Lippincott Williams & Wilkins, 2005, pp. 1045-1066.

Celesia GG, Bodis-Wollner I, Chatrian GE, Harding GF, Sokol S, and Spekreijse H. Recommended standards for electroretinograms and visual evoked potentials. Report of an IFCN committee. *Electroencephalography and Clinical Neurophysiology*, vol. 87, no. 6, pp. 421-436, 1993.

Chiappa K and Hill R. Brainstem auditory evoked potentials: Interpretation. In *Evoked potentials in clinical medicine*, K. Chiappa, Ed., 3rd ed. Philadelphia, Lippincott-Raven, 1997, pp. 199-249.

Crossman AR and Neary D. *Neuroanatomy an illustrated colour text*. 2nd ed. Edinburgh, Churchill Livingstone, 2000.

Cuffin BN. Effects of head shape on EEG's and MEG's. *IEEE Transactions on Biomedical Engineering*, vol. 37, no. 1, pp. 44-52, 1990.

Curio G. Ultrafast EEG activities. In *Electroencephalography: basic principles, clinical application, and related fields*, E. Niedermeyer and F. Lopez da Silva, Eds., 5th ed. Philadelphia, PA, Lippincott Williams & Wilkins, 2005, pp. 495-504.

Darvas F, Ermer JJ, Mosher JC, and Leahy RM. Generic head models for atlas-based EEG source analysis. *Human Brain Mapping*, vol. 27, no. 2, pp. 129-143, 2006.

Davila CE and Mobin MS. Weighted averaging of evoked potentials. *IEEE Transactions on Biomedical Engineering*, vol. 39, no. 4, pp. 338-345, 1992.

Dawson GD. A summation technique for detecting small signals in a large irregular background. *The Journal of Physiology*, vol. 115, no. 1, pp. 2p-3p, 1951.

de Munck JC. The potential distribution in a layered anisotropic spheroidal volume conductor. *Journal of Applied Physics*, vol. 64, no. 2, pp. 464-470, 1988.

de Munck JC, Vijn PC, and Lopes da Silva FH. A random dipole model for spontaneous brain activity. *IEEE Transactions on Biomedical Engineering*, vol. 39, no. 8, pp. 791-804, 1992.

Degen T and Jackel H. A pseudodifferential amplifier for bioelectric events with DC-offset compensation using two-wired amplifying electrodes. *IEEE Transactions on Biomedical Engineering*, vol. 53, no. 2, pp. 300-310, 2006.

Delorme A and Makeig S. EEGLAB: an open source toolbox for analysis of single-trial EEG dynamics including independent component analysis. *Journal of Neuroscience Methods*, vol. 134, no. 1, pp. 9-21, 2004.

Dogdas B, Shattuck DW, and Leahy RM. Segmentation of skull and scalp in 3-D human MRI using mathematical morphology. *Human Brain Mapping*, vol. 26, no. 4, pp. 273-285, 2005.

Don M and Elberling C. Evaluating residual background noise in human auditory brain-stem responses. *The Journal of the Acoustical Society of America*, vol. 96, no. 5 Pt 1, pp. 2746-2757, 1994.

Dössel O and Schneider F. The nullspace of electrocardiography. *Biomedizinische Technik*, vol. 42, Supplement 1, pp. 37-40, 1997.

Dössel O, Schneider F, and Müller M. Optimization of electrode positions in multichannel electrocardiography with respect to electrical imaging of the heart. In the *Proceedings of the 20th Annual Conference of the IEEE Engineering in Medicine and Biology Society*, 1998, pp. 71-74.

Edlinger G, Wach P, and Pfurtscheller G. On the realization of an analytic high-resolution EEG. *IEEE Transactions on Biomedical Engineering*, vol. 45, no. 6, pp. 736-745, 1998.

Elberling C and Don M. Quality estimation of averaged auditory brainstem responses. *Scandinavian audiology*, vol. 13, no. 3, pp. 187-197, 1984.

*Electrical Geodesics, Inc.* [Internet]. Available: http://www.egi.com/c_sales.netshop.html. [accessed 27.10.2006].

*Electrocap International Inc*. [Internet]. Available: http://www.electro-cap.com/. [accessed 27.10.2006].

Fender DH. Models of the human brain and the surrounding media: their influence on the reliability of source localization. *Journal of Clinical Neurophysiology*, vol. 8, no. 4, pp. 381-390, 1991.

Fernandez M and Pallas-Areny R. Ag-AgCl electrode noise in high-resolution ECG measurements. *Biomedical Instrumentation & Technology*, vol. 34, no. 2, pp. 125-130, 2000.

Ferree TC, Eriksen KJ, and Tucker DM. Regional head tissue conductivity estimation for improved EEG analysis. *IEEE Transactions on Biomedical Engineering*, vol. 47, no. 12, pp. 1584-1592, 2000.

Ferree TC, Clay MT, and Tucker DM. The spatial resolution of scalp EEG. *Neurocomputing*, vol. 38-40, pp. 1209-1216, 2001a.

Ferree TC, Luu P, Russell GS, and Tucker DM. Scalp electrode impedance, infection risk, and EEG data quality. *Clinical Neurophysiology*, vol. 112, no. 3, pp. 536-544, 2001b.

Gabriel C, Gabriel S, and Corthout E. The dielectric properties of biological tissues: I. Literature survey. *Physics in Medicine and Biology*, vol. 41, no. 11, pp. 2231-2249, 1996a.

Gabriel S, Lau RW, and Gabriel C. The dielectric properties of biological tissues: II. Measurements in the frequency range 10 Hz to 20 GHz. *Physics in Medicine and Biology*, vol. 41, no. 11, pp. 2251-2269, 1996b.

Geddes LA and Baker LE. The specific resistance of biological material--a compendium of data for the biomedical engineer and physiologist. *Medical & Biological Engineering*, vol. 5, no. 3, pp. 271-293, 1967.

Gencer NG and Williamson SJ. Differential characterization of neural sources with the bimodal truncated SVD pseudo-inverse for EEG and MEG measurements. *IEEE Transactions on Biomedical Engineering*, vol. 45, no. 7, pp. 827-838, 1998.

Geselowitz DB. The concept of equivalent cardiac generator. *Biomedical Sciences Instrumentation*, vol. 1, pp. 325-330, 1963.

Gevins A, Brickett P, Costales B, Le J, and Reutter B. Beyond topographic mapping: towards functional-anatomical imaging with 124-channel EEGs and 3-D MRIs. *Brain Topography*, vol. 3, no. 1, pp. 53-64, 1990.

Gevins A, Le J, Brickett P, Reutter B, and Desmond J. Seeing through the skull: advanced EEGs use MRIs to accurately measure cortical activity from the scalp. *Brain Topography*, vol. 4, no. 2, pp. 125-131, 1991.

Gevins A, Le J, Martin NK, Brickett P, Desmond J, and Reutter B. High resolution EEG: 124-channel recording, spatial deblurring and MRI integration methods. *Electroencephalography and Clinical Neurophysiology*, vol. 90, no. 5, pp. 337-358, 1994.

Gevins A, Leong H, Smith ME, Le J, and Du R. Mapping cognitive brain function with modern high-resolution electroencephalography. *Trends in Neurosciences*, vol. 18, no. 10, pp. 429-436, 1995.

Gevins A, Smith ME, Le J, Leong H, Bennett J, Martin N, McEvoy L, Du R, and Whitfield S. High resolution evoked potential imaging of the cortical dynamics of human working memory. *Electroencephalography and Clinical Neurophysiology*, vol. 98, no. 4, pp. 327-348, 1996.

Gevins A, Le J, Leong H, McEvoy LK, and Smith ME. Deblurring. *Journal of Clinical Neurophysiology*, vol. 16, no. 3, pp. 204-213, 1999.

Golub GH and Van Loan CF. *Matrix computations*. 2nd ed. Baltimore, MD, John Hopkins University Press, 1989.

Goncalves S, de Munck JC, Verbunt JP, Heethaar RM, and Lopes da Silva FH. In vivo measurement of the brain and skull resistivities using an EIT-based method and the combined analysis of SEF/SEP data. *IEEE Transactions on Biomedical Engineering*, vol. 50, no. 9, pp. 1124-1128, 2003a.

Goncalves SI, de Munck JC, Verbunt JP, Bijma F, Heethaar RM, and Lopes da Silva F. In vivo measurement of the brain and skull resistivities using an EIT-based method and realistic models for the head. *IEEE Transactions on Biomedical Engineering*, vol. 50, no. 6, pp. 754-767, 2003b.

Greensite F. Heart surface electrocardiographic inverse solutions. In *Modeling and imaging of bioelectrical activity: principles and applications*, B. He, Ed. New York, Kluwer Academic/Plenum Publishers, 2004, pp. 119-160.

Grieve PG, Emerson RG, Isler JR, and Stark RI. Quantitative analysis of spatial sampling error in the infant and adult electroencephalogram. *Neuroimage*, vol. 21, no. 4, pp. 1260-1274, 2004.

Gutierrez D, Nehorai A, and Muravchik CH. Estimating brain conductivities and dipole source signals with EEG arrays. *IEEE Transactions on Biomedical Engineering*, vol. 51, no. 12, pp. 2113-2122, 2004.

Hallez H, Vanrumste B, Van Hese P, D'Asseler Y, Lemahieu I, and Van de Walle R. A finite difference method with reciprocity used to incorporate anisotropy in electroencephalogram dipole source localization. *Physics in Medicine and Biology*, vol. 50, no. 16, pp. 3787-3806, 2005.

Hansen PC. *Rank-deficient and discrete ill-posed problems: numerical aspects of linear inversion*. Philadelphia, SIAM, 1998.

Haueisen J, Ramon C, Eiselt M, Brauer H, and Nowak H. Influence of tissue resistivities on neuromagnetic fields and electric potentials studied with a finite element model of the head. *IEEE Transactions on Biomedical Engineering*, vol. 44, no. 8, pp. 727-735, 1997.

He B, Wang Y, and Wu D. Estimating cortical potentials from scalp EEG's in a realistically shaped inhomogeneous head model by means of the boundary element method. *IEEE Transactions on Biomedical Engineering*, vol. 46, no. 10, pp. 1264-1268, 1999.

He B, Lian J, and Li G. High-resolution EEG: a new realistic geometry spline Laplacian estimation technique. *Clinical Neurophysiology*, vol. 112, no. 5, pp. 845-852, 2001.

He B, Yao D, and Lian J. High-resolution EEG: on the cortical equivalent dipole layer imaging. *Clinical Neurophysiology*, vol. 113, no. 2, pp. 227-235, 2002a.

He B, Zhang X, Lian J, Sasaki H, Wu D, and Towle VL. Boundary element method-based cortical potential imaging of somatosensory evoked potentials using subjects' magnetic resonance images. *Neuroimage*, vol. 16, no. 3 Pt 1, pp. 564-576, 2002b.

Hjorth B. An on-line transformation of EEG scalp potentials into orthogonal source derivations. *Electroencephalography and Clinical Neurophysiology*, vol. 39, no. 5, pp. 526-530, 1975.

Hoekema R, Wieneke GH, Leijten FS, van Veelen CW, van Rijen PC, Huiskamp GJ, Ansems J, and van Huffelen AC. Measurement of the conductivity of skull, temporarily removed during epilepsy surgery. *Brain Topography*, vol. 16, no. 1, pp. 29-38, 2003.

Huigen E, Peper A, and Grimbergen CA. Investigation into the origin of the noise of surface electrodes. *Medical & Biological Engineering & Computing*, vol. 40, no. 3, pp. 332-338, 2002.

Huiskamp G, Vroeijenstijn M, van Dijk R, Wieneke G, and van Huffelen AC. The need for correct realistic geometry in the inverse EEG problem. *IEEE Transactions on Biomedical Engineering*, vol. 46, no. 11, pp. 1281-1287, 1999.

Hyttinen J. Development of regional aimed ECG leads especially for myocardial ischemia diagnosis. Dissertation. Tampere, Tampere University of Technology, Publication 138, 1994.

Hämäläinen MS and Ilmoniemi RJ. Interpreting magnetic fields of the brain: minimum norm estimates. *Medical & Biological Engineering & Computing*, vol. 32, no. 1, pp. 35-42, 1994.

Im CH, Gururajan A, Zhang N, Chen W, and He B. Spatial resolution of EEG cortical source imaging revealed by localization of retinotopic organization in human primary visual cortex. *Journal of Neuroscience Methods*, vol. 161, no. 1, pp. 142-154, 2007.

Jasper H. Report of the committee on methods of clinical examination in electroencephalography. *Electroencephalography and Clinical Neurophysiology*, vol. 10, no 2., pp. 370-371, 1958.

Kamp A, Pfurtscheller G, Edlinger G, and Lopes da Silva F. Technological basis of EEG recording. In *Electroencephalography: basic principles, clinical application, and related fields*, E. Niedermeyer and F. Lopez da Silva, Eds., 5th ed. Philadelphia, PA, Lippincott Williams & Wilkins, 2005, pp. 127-138.

Kauppinen P, Hyttinen J, Laarne P, and Malmivuo J. A software implementation for detailed volume conductor modelling in electrophysiology using finite difference method. *Computer Methods and Programs in Biomedicine*, vol. 58, no. 2, pp. 191-203, 1999.

Kearfott RB, Sidman RD, Major DJ, and Hill CD. Numerical tests of a method for simulating electrical potentials on the cortical surface. *IEEE Transactions on Biomedical Engineering*, vol. 38, no. 3, pp. 294-299, 1991.

Ko WH. Active electrodes for EEG and evoked potential. In the *Proceedings of the 20th Annual International Conference of the IEEE Engineering in Medicine and Biology Society*, 1998, pp. 2221-2224.

Kosterich JD, Foster KR, and Pollack SR. Dielectric permittivity and electrical conductivity of fluid saturated bone. *IEEE Transactions on Biomedical Engineering*, vol. 30, no. 2, pp. 81-86, 1983.

Laarne P, Eskola H, Hyttinen J, Suihko V, and Malmivuo J. Validation of a detailed computer model for the electric fields in the brain. *Journal of Medical Engineering & Technology*, vol. 19, no. 2-3, pp. 84-87, 1995.

Laarne P, Kauppinen P, Hyttinen J, Malmivuo J, and Eskola H. Effects of tissue resistivities on electroencephalogram sensitivity distribution. *Medical & Biological Engineering & Computing*, vol. 37, no. 5, pp. 555-559, 1999.

Laarne P. Implementation of a realistic conductivity model for the head. Dissertation. Tampere, Tampere University of Technology, Publication 302, 2000.

Lagerlund T and Worrell G. EEG source localization (model-dependent and model-independent methods). In *Electroencephalography: basic principles, clinical application, and related fields*, E. Niedermeyer and F. Lopez da Silva, Eds., 5th ed. Philadelphia, PA, Lippincott Williams & Wilkins, 2005, pp. 829-844.

Lai Y, van Drongelen W, Ding L, Hecox KE, Towle VL, Frim DM, and He B. Estimation of in vivo human brain-to-skull conductivity ratio from simultaneous extra- and intra-cranial electrical potential recordings. *Clinical Neurophysiology*, vol. 116, no. 2, pp. 456-465, 2005.

Lantz G, Grave de Peralta R, Spinelli L, Seeck M, and Michel CM. Epileptic source localization with high density EEG: how many electrodes are needed? *Clinical Neurophysiology*, vol. 114, no. 1, pp. 63-69, 2003.

Law SK. Thickness and resistivity variations over the upper surface of the human skull. *Brain Topography*, vol. 6, no. 2, pp. 99-109, 1993.

Law SK, Nunez PL, and Wijesinghe RS. High-resolution EEG using spline generated surface Laplacians on spherical and ellipsoidal surfaces. *IEEE Transactions on Biomedical Engineering*, vol. 40, no. 2, pp. 145-153, 1993a.

Law SK, Rohrbaugh JW, Adams CM, and Eckardt MJ. Improving spatial and temporal resolution in evoked EEG responses using surface Laplacians. *Electroencephalography and Clinical Neurophysiology*, vol. 88, no. 4, pp. 309-322, 1993b.

Le J and Gevins A. Method to reduce blur distortion from EEG's using a realistic head model. *IEEE Transactions on Biomedical Engineering*, vol. 40, no. 6, pp. 517-528, 1993.

Le J, Menon V, and Gevins A. Local estimate of surface Laplacian derivation on a realistically shaped scalp surface and its performance on noisy data. *Electroencephalography and Clinical Neurophysiology*, vol. 92, no. 5, pp. 433-441, 1994.

Leonowicz Z, Karvanen J, and Shishkin SL. Trimmed estimators for robust averaging of event-related potentials. *Journal of Neuroscience Methods*, vol. 142, no. 1, pp. 17-26, 2005.

Liu AK, Dale AM, and Belliveau JW. Monte Carlo simulation studies of EEG and MEG localization accuracy. *Human Brain Mapping*, vol. 16, no. 1, pp. 47-62, 2002.

Lopes da Silva F. Event-related potentials: methodology and quantification. In *Electroencephalography: basic principles, clinical application, and related fields*, F. Lopez da Silva, Ed., 5th ed. Philadelphia, PA, Lippincott Williams & Wilkins, 2005, pp. 991-1002.

Lopes da Silva F and Van Rotterdam A. Biophysical aspects of EEG and magnetoencephalogram generation. In *Electroencephalography: basic principles, clinical application, and related fields*, E. Niedermeyer and F. Lopez da Silva, Eds., 5th ed. Philadelphia, PA, Lippincott Williams & Wilkins, 2005, pp. 107-126.

Lütkenhöner B. Dipole source localization by means of maximum likelihood estimation. II. Experimental evaluation. *Electroencephalography and Clinical Neurophysiology*, vol. 106, no. 4, pp. 322-329, 1998a.

Lütkenhöner B. Dipole source localization by means of maximum likelihood estimation I. Theory and simulations. *Electroencephalography and Clinical Neurophysiology*, vol. 106, no. 4, pp. 314-321, 1998b.

Malmivuo J and Plonsey R. *Bioelectromagnetism: principles and applications of bioelectric and biomagnetic fields*. New York, Oxford University Press, 1995.

Malmivuo J, Suihko V, and Eskola H. Sensitivity distributions of EEG and MEG measurements. *IEEE Transactions on Biomedical Engineering*, vol. 44, no. 3, pp. 196-208, 1997.

Malmivuo JA and Suihko VE. Effect of skull resistivity on the spatial resolutions of EEG and MEG. *IEEE Transactions on Biomedical Engineering*, vol. 51, no. 7, pp. 1276-1280, 2004.

McFee R and Johnston FD. Electrocardiographic leads. I. Introduction. *Circulation*, vol. 8, no. 4, pp. 554-568, 1953.

McFee R and Johnston FD. Electrocardiographic leads. II. Analysis. *Circulation*, vol. 9, no. 2, pp. 255-266, 1954a.

McFee R and Johnston FD. Electrocardiographic leads. III. Synthesis. *Circulation*, vol. 9, no. 6, pp. 868-880, 1954b.

Meijs JW and Peters MJ. The EEG and MEG, using a model of eccentric spheres to describe the head. *IEEE Transactions on Biomedical Engineering*, vol. 34, no. 12, pp. 913-920, 1987.

Metting van Rijn AC, Peper A, and Grimbergen CA. High-quality recording of bioelectric events. Part 1. Interference reduction, theory and practice. *Medical & Biological Engineering & Computing*, vol. 28, no. 5, pp. 389-397, 1990.

Metting van Rijn AC, Kuiper AP, Dankers TE, and Grimbergen CA. Low-cost active electrode improves the resolution in biopotential recordings. In the *Proceedings of the 18th Annual International Conference of the IEEE Engineering in Medicine and Biology Society*, 1996, pp. 101-102.

Michel CM, Murray MM, Lantz G, Gonzalez S, Spinelli L, and Grave de Peralta R. EEG source imaging. *Clinical Neurophysiology*, vol. 115, no. 10, pp. 2195-2222, 2004.

Mosher JC, Lewis PS, and Leahy RM. Multiple dipole modeling and localization from spatio-temporal MEG data. *IEEE Transactions on Biomedical Engineering*, vol. 39, no. 6, pp. 541-557, 1992.

Mosher JC and Leahy RM. Recursive MUSIC: a framework for EEG and MEG source localization. *IEEE Transactions on Biomedical Engineering*, vol. 45, no. 11, pp. 1342-1354, 1998.

Mosher JC and Leahy RM. Source localization using recursively applied and projected (RAP) MUSIC. *IEEE Transactions on Signal Processing*, vol. 47, no. 2, pp. 332-340, 1999.

Mühler R and von Specht H. Sorted averaging - principle and application to auditory brainstem responses. *Scandinavian Audiology*, vol. 28, no.3, pp. 145-149, 1999.

Neuman MR. Biopotential amplifiers. In *Medical instrumentation: application and design*, J. G. Webster, Ed., 3rd ed. New York, NY, Wiley, 1998, pp. 183-232.

*Neuroscan Quik-Caps*. [Internet]. Available: http://www.neuroscan.com/quick_caps.cfm. [accessed 15.5.2007].

Nicholson PW. Specific impedance of cerebral white matter. *Experimental Neurology*, vol. 13, no. 4, pp. 386-401, 1965.

Niedermeyer E. The normal EEG of the waking adult. In *Electroencephalography: basic principles, clinical application, and related fields*, E. Niedermeyer and F. Lopez da Silva, Eds., 5th ed. Philadelphia, PA, Lippincott Williams & Wilkins, 2005a, pp. 167-192.

Niedermeyer E. Historical aspects. In *Electroencephalography: basic principles, clinical application, and related fields*, E. Niedermeyer and F. Lopez da Silva, Eds., 5th ed. Philadelphia, PA, Lippincott Williams & Wilkins, 2005b, pp. 1-16.

Nunez PL, Silberstein RB, Cadusch PJ, Wijesinghe RS, Westdorp AF, and Srinivasan R. A theoretical and experimental study of high resolution EEG based on surface Laplacians and cortical imaging. *Electroencephalography and Clinical Neurophysiology*, vol. 90, no. 1, pp. 40-57, 1994.

Nunez PL, Srinivasan R, Westdorp AF, Wijesinghe RS, Tucker DM, Silberstein RB, and Cadusch PJ. EEG coherency. I: statistics, reference electrode, volume conduction, Laplacians, cortical imaging, and interpretation at multiple scales. *Electroencephalography and Clinical Neurophysiology*, vol. 103, no. 5, pp. 499-515, 1997.

Nunez PL, Silberstein RB, Shi Z, Carpenter MR, Srinivasan R, Tucker DM, Doran SM, Cadusch PJ, and Wijesinghe RS. EEG coherency II: experimental comparisons of multiple measures. *Clinical Neurophysiology*, vol. 110, no. 3, pp. 469-486, 1999.

Nunez PL and Srinivasan R. *Electric fields of the brain: the neurophysics of EEG*. 2nd ed. New York, Oxford University Press, 2006.

Nuwer MR, Aminoff M, Goodin D, Matsuoka S, Mauguière F, Starr A, and Vibert JF. IFCN recommended standards for brain-stem auditory evoked potentials. Report of an IFCN committee. International Federation of Clinical Neurophysiology. *Electroencephalography and Clinical Neurophysiology*, vol. 91, no. 1, pp. 12-17, 1994.

Ollikainen JO, Vauhkonen M, Karjalainen PA, and Kaipio JP. A new computational approach for cortical imaging. *IEEE Transactions on Medical Imaging*, vol. 20, no. 4, pp. 325-332, 2001.

Olson WH. Basic concepts of medical instrumentation. In *Medical instrumentation: application and design*, J. G. Webster, Ed., 3rd ed. New York, NY, Wiley, 1998, pp. 1-43.

Oostendorp TF, Delbeke J, and Stegeman DF. The conductivity of the human skull: results of in vivo and in vitro measurements. *IEEE Transactions on Biomedical Engineering*, vol. 47, no. 11, pp. 1487-1492, 2000.

Oostenveld R and Praamstra P. The five percent electrode system for high-resolution EEG and ERP measurements. *Clinical Neurophysiology*, vol. 112, no. 4, pp. 713-719, 2001.

Pascual-Marqui RD, Michel CM, and Lehmann D. Low resolution electromagnetic tomography: a new method for localizing electrical activity in the brain. *International Journal of Psychophysiology*, vol. 18, no. 1, pp. 49-65, 1994.

Perrin F, Bertrand O, and Pernier J. Scalp current density mapping: value and estimation from potential data. *IEEE Transactions on Biomedical Engineering*, vol. 34, no. 4, pp. 283-288, 1987.

Plonsey R and Heppner DB. Considerations of quasi-stationarity in electrophysiological systems. *The Bulletin of Mathematical Biophysics*, vol. 29, no. 4, pp. 657-664, 1967.

Pohlmeier R, Buchner H, Knoll G, Rienäcker A, Beckmann R, and Pesch J. The influence of skull-conductivity misspecification on inverse source localization in realistically shaped finite element head models. *Brain Topography*, vol. 9, no. 3, pp. 157-162, 1997.

*Polhemus*. [Internet]. Available: http://www.polhemus.com/?page=Motion_Fastrak. [accessed 28.3.2008].

Quesney L and Niedermeyer E. Electrocortigography. In *Electroencephalography: basic principles, clinical application, and related fields*, E. Niedermeyer and F. Lopez da Silva, Eds., 5th ed. Philadelphia, PA, Lippincott Williams & Wilkins, 2005, pp. 769-775.

Ramon C, Schimpf P, Haueisen J, Holmes M, and Ishimaru A. Role of soft bone, CSF and gray matter in EEG simulations. *Brain Topography*, vol. 16, no. 4, pp. 245-248, 2004.

Ramon C, Schimpf P, and Haueisen J. Influence of head models on EEG simulations and inverse source localizations. *Biomedical Engineering Online*, vol. 5, no. 10, 2006.

Raz J, Turetsky B, and Fein G. Confidence intervals for the signal-to-noise ratio when a signal embedded in noise is observed over repeated trials. *IEEE Transactions on Biomedical Engineering*, vol. 35, no. 8, pp. 646-649, 1988.

Rush S and Driscoll DA. Current distribution in the brain from surface electrodes. *Anesthesia and Analgesia*, vol. 47, no. 6, pp. 717-723, 1968.

Rush S and Driscoll DA. EEG electrode sensitivity--an application of reciprocity. *IEEE Transactions on Biomedical Engineering*, vol. 16, no. 1, pp. 15-22, 1969.

Russell GS, Jeffrey Eriksen K, Poolman P, Luu P, and Tucker DM. Geodesic photogrammetry for localizing sensor positions in dense-array EEG. *Clinical Neurophysiology*, vol. 116, no. 5, pp. 1130-1140, 2005.

Sadleir RJ and Argibay A. Modeling skull electrical properties. *Annals of Biomedical Engineering*, vol. 35, no. 10, pp. 1699-1712, 2007.

Scheer HJ, Sander T, and Trahms L. The influence of amplifier, interface and biological noise on signal quality in high-resolution EEG recordings. *Physiological Measurement*, vol. 27, no. 2, pp. 109-117, 2006.

Scherg M and von Cramon D. A new interpretation of the generators of BAEP waves I-V: results of a spatio-temporal dipole model. *Electroencephalography and Clinical Neurophysiology*, vol. 62, no. 4, pp. 290-299, 1985.

Scherg M and Von Cramon D. Evoked dipole source potentials of the human auditory cortex. *Electroencephalography and Clinical Neurophysiology*, vol. 65, no. 5, pp. 344-360, 1986.

Schneider F, Dössel O, and Müller M. Filtering characteristics of the human body and reconstruction limits in the inverse problem of electrocardiography. *Computers in Cardiology*, vol. 25, pp. 689-692, 1998.

Schneider F. Das inverse Problem der Elektro- und Magnetokardiographie - Optimale Erfassung und Nutzung der messbaren Information. Dissertation. Karlsruhe, Univerität Karlsruhe(TH), 1999.

Shibasaki H. Human brain mapping: Hemodynamic response and electrophysiology. *Clinical Neurophysiology*, vol. 119, no. 4, pp. 731-743, 2008.

Sidman RD, Vincent DJ, Smith DB, and Lee L. Experimental tests of the cortical imaging technique--applications to the response to median nerve stimulation and the localization of epileptiform discharges. *IEEE Transactions on Biomedical Engineering*, vol. 39, no. 5, pp. 437-444, 1992.

Skipa O, 2002. Comments on the null-space of electrocardiography. Personal communication.

Srebro R, Oguz RM, Hughlett K, and Purdy PD. Estimating regional brain activity from evoked potential fields on the scalp. *IEEE Transactions on Biomedical Engineering*, vol. 40, no. 6, pp. 509-516, 1993.

Srinivasan R, Nunez PL, Tucker DM, Silberstein RB, and Cadusch PJ. Spatial sampling and filtering of EEG with spline laplacians to estimate cortical potentials. *Brain Topography*, vol. 8, no. 4, pp. 355-366, 1996.

Srinivasan R, Tucker DM, and Murias M. Estimating the spatial Nyquist of the human EEG. *Behavior Research Methods, Instruments, & Computers*, vol. 30, no. 1, pp. 8-19, 1998.

Srinivasan R, Winter WR, Ding J, and Nunez PL. EEG and MEG coherence: measures of functional connectivity at distinct spatial scales of neocortical dynamics. *Journal of Neuroscience Methods*, vol. 166, no. 1, pp. 41-52, 2007.

Sörnmo L and Laguna P. *Bioelectrical signal processing in cardiac and neurological applications*. New York, Academic press, 2005.

Takano N. Reduction of ECG leads and equivalent sources using orthogonalization and clustering techniques. Dissertation. Tampere, Tampere University of Technology, Publication 382, 2002.

Tucker DM. Spatial sampling of head electrical fields: the geodesic sensor net. *Electroencephalography and Clinical Neurophysiology*, vol. 87, no. 3, pp. 154-163, 1993.

Walker SJ. Epicardial potential distributions calculated from body surface measurements using multiple torso models. Dissertation. University of Tasmania, 1985.

Walker SJ and Kilpatrick D. Forward and inverse electrocardiographic calculations using resistor network models of the human torso. *Circulation Research*, vol. 61, no. 4, pp. 504-513, 1987.

van Drongelen W, Yuchtman M, Van Veen BD, and van Huffelen AC. A spatial filtering technique to detect and localize multiple sources in the brain. *Brain Topography*, vol. 9, no. 1, pp. 39-49, 1996.

Van Veen BD, and Buckley KM. Beamforming: A versatile approach to spatial filtering. IEEE ASSP Magazine, vol. 5, no.2 ,pp.4-24, 1988.

Van Veen BD, van Drongelen W, Yuchtman M, and Suzuki A. Localization of brain electrical activity via linearly constrained minimum variance spatial filtering. *IEEE Transactions on Biomedical Engineering*, vol. 44, no. 9, pp. 867-880, 1997.

Wang Y and He B. A computer simulation study of cortical imaging from scalp potentials. *IEEE Transactions on Biomedical Engineering*, vol. 45, no. 6, pp. 724-735, 1998.

Vanrumste B, Van Hoey G, Van de Walle R, D'Have MR, Lemahieu IA, and Boon PA. Comparison of performance of spherical and realistic head models in dipole localization from noisy EEG. *Medical Engineering & Physics*, vol. 24, no. 6, pp. 403-418, 2002.

Ward DM, Jones RD, Bones PJ, and Carroll GJ. Enhancement of deep epileptiform activity in the EEG via 3-D adaptive spatial filtering. *IEEE Transactions on Biomedical Engineering*, vol. 46, no. 6, pp. 707-716, 1999.

Wendel K, Narra NG, Hannula M, Kauppinen P, and Malmivuo J. The influence of CSF on EEG sensitivity distributions of multilayered head models. *IEEE Transactions on Biomedical Engineering*, vol. 55, no. 4, pp. 1454-1456, 2008.

Wikswo JP, Jr., Gevins A, and Williamson SJ. The future of the EEG and MEG. *Electroencephalography and Clinical Neurophysiology*, vol. 87, no. 1, pp. 1-9, 1993.

Wolters CH, Anwander A, Tricoche X, Weinstein D, Koch MA, and MacLeod RS. Influence of tissue conductivity anisotropy on EEG/MEG field and return current computation in a realistic head model: a simulation and visualization study using high-resolution finite element modeling. *Neuroimage*, vol. 30, no. 3, pp. 813-826, 2006.

Yamashita Y. Theoretical studies on the inverse problem in electrocardiography and the uniqueness of the solution. *IEEE Transactions on Biomedical Engineering*, vol. 29, no. 11, pp. 719-725, 1982.

Yamashita Y and Takahashi T. Use of the finite element method to determine epicardial from body surface potentials under a realistic torso model. *IEEE Transactions on Biomedical Engineering*, vol. 31, no. 9, pp. 611-621, 1984.

Yao J and Dewald JP. Evaluation of different cortical source localization methods using simulated and experimental EEG data. *Neuroimage*, vol. 25, no. 2, pp. 369-382, 2005.

Zhang X, van Drongelen W, Hecox KE, Towle VL, Frim DM, McGee AB, and He B. High-resolution EEG: cortical potential imaging of interictal spikes. *Clinical Neurophysiology*, vol. 114, no. 10, pp. 1963-1973, 2003.

Zhang Y, Ding L, van Drongelen W, Hecox K, Frim DM, and He B. A cortical potential imaging study from simultaneous extra- and intracranial electrical recordings by means of the finite element method. *Neuroimage*, vol. 31, no. 4, pp. 1513-1524, 2006a.

Zhang Y, van Drongelen W, and He B. Estimation of in vivo brain-to-skull conductivity ratio in humans. *Applied Physics Letters*, vol. 89, no. 22, pp. 3p, 2006b.

Özdamar Ö and Kalayci T. Median averaging of auditory brain stem responses. *Ear and Hearing*, vol. 20, no. 3, pp. 253-264, 1999.

# 9 ORIGINAL PUBLICATIONS